Missouri University of Science and Technology
Scholars' Mine

Mathematics and Statistics Faculty Research & Creative Works

Mathematics and Statistics

25 Dec 2013

Efficient and Long-Time Accurate Second-Order Methods for the Stokes-Darcy System

Wenbin Chen

Max Gunzburger

Dong Sun

Xiaoming Wan
Missouri University of Science and Technology, xiaomingwang@mst.edu

Follow this and additional works at: https://scholarsmine.mst.edu/math_stat_facwork

 Part of the Mathematics Commons, and the Statistics and Probability Commons

Recommended Citation

W. Chen et al., "Efficient and Long-Time Accurate Second-Order Methods for the Stokes-Darcy System," *SIAM Journal on Numerical Analysis*, vol. 51, no. 5, pp. 2563 - 2584, Society for Industrial and Applied Mathematics, Dec 2013.
The definitive version is available at https://doi.org/10.1137/120897705

This Article - Journal is brought to you for free and open access by Scholars' Mine. It has been accepted for inclusion in Mathematics and Statistics Faculty Research & Creative Works by an authorized administrator of Scholars' Mine. This work is protected by U. S. Copyright Law. Unauthorized use including reproduction for redistribution requires the permission of the copyright holder. For more information, please contact scholarsmine@mst.edu.

SIAM J. NUMER. ANAL.
Vol. 51, No. 5, pp. 2563–2584
© 2013 Society for Industrial and Applied Mathematics

EFFICIENT AND LONG-TIME ACCURATE SECOND-ORDER METHODS FOR THE STOKES–DARCY SYSTEM*

WENBIN CHEN†, MAX GUNZBURGER‡, DONG SUN§, AND XIAOMING WANG§

Abstract. We propose and study two second-order in time implicit-explicit methods for the coupled Stokes–Darcy system that governs flows in karst aquifers and other subsurface flow systems. The first method is a combination of a second-order backward differentiation formula and the second-order Gear's extrapolation approach. The second is a combination of the second-order Adams–Moulton and second-order Adams–Bashforth methods. Both algorithms only require the solution of *decoupled* Stokes and Darcy problems at each time-step. Hence, these schemes are very efficient and can be easily implemented using legacy codes. We establish the unconditional and uniform in time stability for both schemes. The uniform in time stability leads to uniform in time control of the error which is highly desirable for modeling physical processes, e.g., contaminant sequestration and release, that occur over very long time scales. Error estimates for fully discretized schemes using finite element spatial discretizations are derived. Numerical examples are provided that illustrate the accuracy, efficiency, and long-time stability of the two schemes.

Key words. Stokes–Darcy systems, backward differentiation formulas, Gear's extrapolation, Adams–Moulton and Adams–Bashforth methods, unconditional stability, long-time stability, uniform in time error estimates, finite element methods, karst aquifers

AMS subject classifications. 35M13, 35Q35, 65N30, 65N55, 76D07, 76S05

DOI. 10.1137/120897705

1. Introduction.

Karst is a common type of landscape formed by the dissolution of layers of soluble bedrock, usually including carbonate rock, limestone, and dolomite. Karst regions often contain karst aquifers, which are important sources of potable water. For example, about 90% of the fresh water used in Florida comes from karst aquifers [27]. Clearly, the study of karst aquifers is of great importance, especially because they are seriously threatened by contamination [29].

A karst aquifer, in addition to a porous limestone or dolomite matrix, typically has large cavernous conduits that are known to have great impact on groundwater flow and contaminant transport within the aquifer. During high-rain seasons, the water pressure in the conduits is larger than that in the ambient matrix so that conduit-borne contaminants can be driven into the matrix. During dry seasons, the pressure differential reverses and contaminants long sequestered in the matrix can be released into the free flow in the conduits and exit through, e.g., springs and wells, into surface water systems. Therefore, an understanding of the interaction between the free flow in the conduits and the Darcy flow in the matrix is crucial to the study of groundwater flows and contaminant transport in karst regions.

*Received by the editors November 5, 2012; accepted for publication (in revised form) June 25, 2013; published electronically September 10, 2013. This work was supported in part by the National Science Foundation through DMS10008852, a planning grant from Florida State University, the Ministry of Education of China and the State Administration of Foreign Experts Affairs of China under a 111 project grant (B08018), and the Natural Science Foundation of China under grant 11171077.

http://www.siam.org/journals/sinum/51-5/89770.html

†School of Mathematical Sciences, Fudan University, Shanghai 200433, China (wbchen@fudan.edu.cn).

‡Department of Scientific Computing, Florida State University, Tallahassee, FL 32306-4120 (gunzburg@fsu.edu).

§Department of Mathematics, Florida State University, Tallahassee, FL 32306 (dsun@math.fsu.edu, wxm@math.fsu.edu).

Copyright © by SIAM. Unauthorized reproduction of this article is prohibited.

Downloaded 03/17/23 to 131.151.26.204 . Redistribution subject to SIAM license or copyright; see https://epubs.siam.org/terms-privacy

Downloaded 03/17/23 to 131.151.26.204 . Redistribution subject to SIAM license or copyright; see https://epubs.siam.org/terms-privacy

The mathematical study of flows in karst aquifers is a well-known challenge due to the coupling of the flow in the conduits and the flow in the surrounding matrix, the complex geometry of the network of conduits, the vastly disparate spatial and temporal scales, the strong heterogeneity of the physical parameters, and the huge associated uncertainties in the data. Even for a small, lab-size conceptual model with only one conduit (pipe) embedded in a homogeneous porous media (matrix), significant mathematically rigorous progress has only recently been achieved. For the coupled Stokes–Darcy model that includes the classical Beavers–Joseph [6] matrix-conduit interface boundary condition, see [7, 8, 9]. For various simplified interface conditions, see, e.g., [7, 17, 25, 30]. Nonlinear interface conditions have also been proposed for Navier–Stokes/Darcy modeling; see, e.g., [11, 19].

Due to the practical importance of the problem of flow and contaminant transport in karst aquifers, there has been a lot of attention recently on the development of accurate and efficient numerical methods for the coupled Stokes–Darcy system; see, e.g., [10, 17, 30, 36] among many others. The efficiency of the algorithms is a particularly important issue due to the large scale of field applications. Because of the disparity of governing equations and physics in the conduit and matrix, domain decomposition methods (also called partitioned methods by some authors) that only require separate Stokes and Darcy solves seem natural; see, e.g., [12, 13, 17, 18, 28, 31, 32, 33, 37, 38]. On the other hand, long-time accuracy of the schemes is also highly desirable because the physical phenomena of retention and release of contaminants takes place over a very long time scale. Therefore, there is a need to ensure the long-time accuracy of the discretization algorithms in addition to the standard notion of accuracy on an order one time scale.

The purpose of this work is to propose and investigate two types of numerical methods for the coupled Stokes–Darcy system. We discretize the system in time via either a combination of a second-order backward-differentiation formula and Gear extrapolation methods or a combination of second-order Adams–Moulton and Adams–Bashforth methods. These algorithms are special cases of the implicit-explicit (IMEX) class of schemes [1, 2, 3, 4, 5, 20]. The coupling terms in the interface conditions are treated explicitly in our algorithm so that only two decoupled problems (one Stokes and one Darcy) are solved at each time-step. Therefore, these schemes can be implemented very efficiently and, in particular, legacy codes for each of the two components can be utilized. Moreover, we show that despite the explicit treatment of the coupling terms, our schemes are unconditionally stable and long-time stable in the sense that the solutions remain uniformly bounded in time. The uniform in time bound of the solution further leads to uniform in time error estimates. This is a highly desirable feature because one would want to have reliable numerical results over the long time scale of contaminant sequestration and release. Uniform in time error estimates for fully discrete schemes using finite element spatial discretizations are also presented. Our numerical experiments illustrate our analytical results.

Our work can be viewed as a time-dependent noniterative version of the steady-state domain decomposition work in [13, 17] and as a generalization of the first-order schemes in [10, 37] that achieve the desirable second-order accuracy without increasing the complexity. The backward differentiation–based algorithm can be viewed as an infinite-dimensional version of the scheme presented in [33], but with the additional important result on time-uniform error estimates. The Adams–Moulton/Bashford based algorithm is new so far as the Stokes–Darcy problem is concerned. To the best of our knowledge, our uniform in time error estimates are among the first of their kind for Stokes–Darcy and related systems.

Copyright © by SIAM. Unauthorized reproduction of this article is prohibited.

Downloaded 03/17/23 to 131.151.26.204 . Redistribution subject to SIAM license or copyright; see https://epubs.siam.org/terms-privacy

The rest of the paper is organized as follows. In section 2, we introduce the coupled Stokes–Darcy system and the associated weak formulation as well as the two second-order in time schemes. The unconditional and long-time stability with respect to the L^2-norm are presented in section 3. Section 4 is devoted to the stability with respect to the H^1-norm. The H^1 estimates are important for the finite element analysis; this is another new feature of our work, even for first-order schemes. In section 5, we focus on the error analysis of the fully discretized scheme using finite element spatial discretizations. Numerical results that illustrate the accuracy, efficiency, and long-time stability of our our algorithms are given in section 6. We close by providing some concluding remarks in section 7.

2. The Stokes–Darcy system and two types of IMEX methods.

2.1. The Stokes–Darcy system. For simplicity, we consider a conceptual domain for a karst aquifer that consists of a porous media (matrix), denoted by $\Omega_p \in \mathbb{R}^d$, and a conduit, denoted by $\Omega_f \in \mathbb{R}^d$, where $d = 2, 3$ denotes the spatial dimension. The interface between the matrix and the conduit is denoted Γ. The remaining parts of the boundaries of Ω_p and Ω_f are denoted by $\partial\Omega_p$ and $\partial\Omega_f$, respectively. See Figure 2.1.

The coupled Stokes–Darcy system governing fluid flow in the karst system is given by [7, 17]

$$\begin{cases} S\dfrac{\partial \phi}{\partial t} - \nabla \cdot (\mathbb{K}\nabla\phi) = f & \text{in } \Omega_p, \\ \dfrac{\partial \mathbf{u}_f}{\partial t} - \nabla \cdot \mathbb{T}(\mathbf{u}_f, p) = \mathbf{f} \quad \text{and} \quad \nabla \cdot \mathbf{u}_f = 0 & \text{in } \Omega_f, \end{cases} \tag{2.1}$$

where the unknowns are the fluid velocity $\mathbf{u}_f$ and the kinematic pressure p in the conduit and the hydraulic head ϕ in the matrix; the velocity in the matrix is recovered from $\mathbf{u}_p = -\mathbb{K}\nabla\phi$. In (2.1), $\mathbf{f}$ and f denote external body forces acting on the domains Ω_f and Ω_p, respectively, and $\mathbb{T}(\mathbf{v}, p) = \nu(\nabla\mathbf{v} + \nabla^T\mathbf{v}) - p\mathbb{I}$ denotes the stress tensor. The parameters appearing in (2.1) are the water storage coefficient S, the hydraulic conductivity tensor $\mathbb{K}$, and the kinematic viscosity of the fluid ν.

For simplicity, we assume homogeneous Dirichlet boundary conditions for the hydraulic head and fluid velocity on the outer boundaries $\partial\Omega_p$ and $\partial\Omega_f$, respectively. On the interface Γ, we impose the *Beavers–Joseph–Saffman–Jones interface conditions* [6, 26, 39]

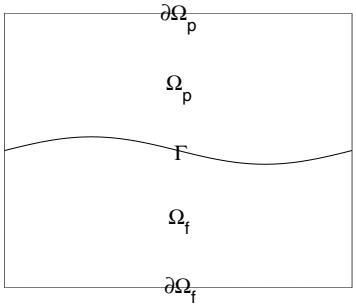

FIG. 2.1. *The physical domain consisting of a porous media Ω_p and a free-flow conduit Ω_f.*

Copyright © by SIAM. Unauthorized reproduction of this article is prohibited.

$$\begin{cases} \mathbf{u}_f \cdot \mathbf{n}_f = \mathbf{u}_p \cdot \mathbf{n}_f = -(\mathbb{K}\nabla\phi) \cdot \mathbf{n}_f, \\ -\boldsymbol{\tau}_j \cdot (\mathbb{T}(\mathbf{u}_f, p_f) \cdot \mathbf{n}_f) = \alpha_{BJSJ} \boldsymbol{\tau}_j \cdot \mathbf{u}_f, \quad j = 1, \ldots, d-1, \\ -\mathbf{n}_f \cdot (\mathbb{T}(\mathbf{u}_f, p_f) \cdot \mathbf{n}_f) = g\phi, \end{cases} \tag{2.2}$$

where $\mathbf{n}_f$ denotes the outer unit normal vector for Ω_f and $\{\boldsymbol{\tau}_j\}_{j=1,2,\ldots,d-1}$ denotes a linearly independent set of vectors tangent to the interface Γ. The additional parameters appearing in (2.2) are the gravitational constant g and the Beavers–Joseph–Saffman–Jones coefficient α_{BJSJ}.

2.2. Weak formulation. We denote by $(\cdot,\cdot)_D$ and $\|\cdot\|_D$ the standard $L^2(D)$ inner product and norm, respectively, where D may be Ω_f, Ω_p, or Γ. We often suppress the subscript D if there is no possibility of confusion. We define the spaces

$$\begin{aligned} \mathbf{H}_f &= \left\{ \mathbf{v} \in \left(H^1(\Omega_f)\right)^d \;\mid\; \mathbf{v} = \mathbf{0} \text{ on } \partial\Omega_f \setminus \Gamma \right\}, \\ H_p &= \left\{ \psi \in H^1(\Omega_p) \;\mid\; \psi = 0 \text{ on } \partial\Omega_p \setminus \Gamma \right\}, \\ Q &= L^2(\Omega_f), \qquad \mathbf{W} = \mathbf{H}_f \times H_p. \end{aligned}$$

Dual spaces are denoted by $(\cdot)'$ and duality parings between spaces and their duals induced by the L^2 inner product on the appropriate domain are denoted by $\langle \cdot, \cdot \rangle$.

A weak formulation of the Stokes–Darcy system (2.1) is derived by multiplying the three equations in that system by test functions $\mathbf{v} \in \mathbf{H}_f$, $g\psi \in \mathbf{H}_p$, and $q \in Q$, respectively, then integrating over the corresponding domains, then integrating by parts the terms involving second-derivative operators, and then substituting the interface conditions (2.2) in the appropriate terms. The resulting weak formulation is given as follows [7, 16]: given $f \in (H_p)'$ and $\mathbf{F} \in (\mathbf{H}_f)'$, seek $\phi \in H_p$, $\mathbf{u}_f \in \mathbf{H}_f$, and $p \in Q$, with $\partial\phi/\partial t \in (H_p)'$ and $\partial\mathbf{u}/\partial t \in (\mathbf{H}_f)'$, satisfying

$$\begin{aligned} \langle\langle \vec{\mathbf{u}}_t, \vec{\mathbf{v}} \rangle\rangle + a(\vec{\mathbf{u}}, \vec{\mathbf{v}}) + b(\mathbf{v}, p) + a_\Gamma(\vec{\mathbf{u}}, \vec{\mathbf{v}}) &= \langle\langle \langle \vec{\mathbf{f}}, \vec{\mathbf{v}} \rangle\rangle\rangle, \\ b(\mathbf{u}, q) &= 0, \end{aligned} \tag{2.3}$$

where $\vec{\mathbf{u}} = [\mathbf{u}, \phi]^T$, $\vec{\mathbf{v}} = [\mathbf{v}, \psi]^T$, and $\vec{\mathbf{f}} = [\mathbf{f}, gf]^T$ and where $(\cdot)_t = \partial(\cdot)/\partial t$. In (2.3), we have that

$$\begin{aligned} \langle\langle \vec{\mathbf{u}}_t, \vec{\mathbf{v}} \rangle\rangle &= \langle \mathbf{u}_t, \mathbf{v} \rangle_{\Omega_f} + gS \langle \phi_t, \psi \rangle_{\Omega_p}, \qquad b(\mathbf{v}, q) = -(q, \nabla \cdot \mathbf{v})_{\Omega_f} \\ a(\vec{\mathbf{u}}, \vec{\mathbf{v}}) &= a_f(\mathbf{u}, \mathbf{v}) + a_p(\phi, \psi) + a_{BJSJ}(\mathbf{u}, \mathbf{v}), \\ a_\Gamma(\vec{\mathbf{u}}, \vec{\mathbf{v}}) &= g(\phi, \mathbf{v} \cdot \mathbf{n}_f)_\Gamma - g(\mathbf{u} \cdot \mathbf{n}_f, \psi)_\Gamma, \quad \langle\langle \langle \vec{\mathbf{f}}, \vec{\mathbf{v}} \rangle\rangle\rangle = \langle \mathbf{f}, \mathbf{v} \rangle_{\Omega_f} + g \langle f, \psi \rangle_{\Omega_p}, \end{aligned} \tag{2.4}$$

where

$$\begin{aligned} a_f(\mathbf{u}, \mathbf{v}) = \nu(\nabla\mathbf{u}, \nabla\mathbf{v})_{\Omega_f}, \qquad a_p(\phi, \psi) = g(\mathbb{K}\nabla\phi, \nabla\psi)_{\Omega_p}, \\ a_{BJSJ}(\mathbf{u}, \mathbf{v}) = \alpha_{BJSJ}(\mathbf{u} \cdot \vec{\tau}, \mathbf{v} \cdot \vec{\tau})_\Gamma. \end{aligned}$$

In (2.3), $\mathbf{u}_f$, ϕ, and p are the primary variables; as mentioned, once the hydraulic head ϕ is known, one can recover $\mathbf{u}_p$, the velocity in the porous media, via the Darcy relation $\mathbf{u}_p = -\mathbf{K}\nabla\phi$.

It can be shown that the bilinear form $a(\cdot,\cdot)$ is *coercive*; indeed, we have that [7]

$$a(\vec{\mathbf{u}}, \vec{\mathbf{u}}) \geq (\nu \|\nabla\mathbf{u}\|^2 + gK_{\min}\|\nabla\phi\|^2 + \alpha_{BJSJ}\|\mathbf{u} \cdot \vec{\tau}\|_\Gamma^2) \geq C_a \|\nabla\vec{\mathbf{u}}\|^2, \tag{2.5}$$

Copyright © by SIAM. Unauthorized reproduction of this article is prohibited.

Downloaded 03/17/23 to 131.151.26.204 . Redistribution subject to SIAM license or copyright; see https://epubs.siam.org/terms-privacy

Downloaded 03/17/23 to 131.151.26.204 . Redistribution subject to SIAM license or copyright; see https://epubs.siam.org/terms-privacy

where $C_a = \min(\nu, gK_{\min}) > 0$ and where $K_{\min}$ denotes the smallest eigenvalue of $\mathbb{K}$. We define the norms $\|\vec{\mathbf{u}}\|_a = a(\vec{\mathbf{u}}, \vec{\mathbf{u}})^{\frac{1}{2}}$ and $\|\vec{\mathbf{v}}\|_S = \langle\langle \vec{\mathbf{v}}, \vec{\mathbf{v}} \rangle\rangle^{\frac{1}{2}}$. We have that $\|\vec{\mathbf{v}}\|_S$ is equivalent to the L^2-norm, i.e., we have that

$$c_s \|\vec{\mathbf{v}}\|_S \le \|\vec{\mathbf{v}}\| \le C_S \|\vec{\mathbf{v}}\|_S. \tag{2.6}$$

where $c_s = \min\{1, gS\} > 0$ and $C_S = \max\{1, gS\} > 0$.

2.3. The second-order backward-differentiation scheme (BDF2). The first scheme we introduce discretizes in time via a second-order backward-differentiation formula (BDF), where the interface term is treated via a second-order explicit Gear's extrapolation formula. We propose the following algorithm: for any $\vec{\mathbf{v}} \in \mathbf{W}$ and $q \in Q$,

$$\begin{aligned} &\left\langle\left\langle \frac{3\vec{\mathbf{u}}^{n+1} - 4\vec{\mathbf{u}}^n + \vec{\mathbf{u}}^{n-1}}{2\Delta t}, \vec{\mathbf{v}} \right\rangle\right\rangle + a(\vec{\mathbf{u}}^{n+1}, \vec{\mathbf{v}}) + b(\mathbf{v}, p^{n+1}) + a_{st}(\vec{\mathbf{u}}^{n+1}, \vec{\mathbf{v}}) \\ &\qquad = \langle\langle \vec{\mathbf{f}}^{n+1}, \vec{\mathbf{v}} \rangle\rangle - \widetilde{a}_\Gamma(2\vec{\mathbf{u}}^n - \vec{\mathbf{u}}^{n-1}, \vec{\mathbf{v}}), \\ &b(\mathbf{u}^{n+1}, q) = 0, \end{aligned} \tag{2.7}$$

where the artificial stabilizing term $a_{st}(\cdot, \cdot)$ is defined as

$$a_{st}(\vec{\mathbf{u}}, \vec{\mathbf{v}}) = \gamma_f(\mathbf{u} \cdot \mathbf{n}_f, \mathbf{v} \cdot \mathbf{n}_f)_\Gamma + \gamma_p(\phi, \psi)_\Gamma \tag{2.8}$$

with parameters $\gamma_f, \gamma_p \ge 0$ and $\widetilde{a}_\Gamma(\vec{\mathbf{u}}, \vec{\mathbf{v}})$ is defined as

$$\widetilde{a}_\Gamma(\vec{\mathbf{u}}, \vec{\mathbf{v}}) = a_\Gamma(\vec{\mathbf{u}}, \vec{\mathbf{v}}) - a_{st}(\vec{\mathbf{u}}, \vec{\mathbf{v}}).$$

2.4. The second-order Adams–Moulton–Bashforth method (AMB2). For the second scheme, we combine the second-order implicit Adams–Moulton treatment of the symmetric terms and the second-order explicit Adams–Bashforth treatment of the interface term to propose the following second-order scheme: for any $\vec{\mathbf{v}} \in \mathbf{W}$ and $q \in Q$,

$$\begin{aligned} &\left\langle\left\langle \frac{\vec{\mathbf{u}}^{n+1} - \vec{\mathbf{u}}^n}{\Delta t}, \vec{\mathbf{v}} \right\rangle\right\rangle + a\left(D_\alpha \vec{\mathbf{u}}^{n+1}, \vec{\mathbf{v}}\right) + b\left(\mathbf{v}, D_\alpha p^{n+1}\right) + a_{st}\left(D_\alpha \vec{\mathbf{u}}^{n+1}, \vec{\mathbf{v}}\right) \\ &\qquad = \langle\langle \vec{\mathbf{f}}^{n+\frac{1}{2}}, \vec{\mathbf{v}} \rangle\rangle - \widetilde{a}_\Gamma\left(\frac{3}{2}\vec{\mathbf{u}}^n - \frac{1}{2}\vec{\mathbf{u}}^{n-1}, \vec{\mathbf{v}}\right), \\ &b\left(D_\alpha \mathbf{u}^{n+1}, q\right) = 0, \end{aligned} \tag{2.9}$$

where D_α denotes the difference operator that depends on a parameter α and is defined by $D_\alpha v^{n+1} = \alpha v^{n+1} + \left(\frac{3}{2} - 2\alpha\right) v^n + \left(\alpha - \frac{1}{2}\right) v^{n-1}$. The stabilizing term $a_{st}(\cdot, \cdot)$ is defined as in (2.8).

In the analysis, we have not taken advantage of the stabilizing term, but the numerical experiments in section 6 demonstrate the stabilizing effects in the sense that the presence of the stabilizing term relaxes the time-step restriction.

2.5. Efficiency of the schemes. The implemented schemes are highly efficient because we can decouple the Stokes and Darcy subproblems:

1. given $\vec{\mathbf{u}}^n, \vec{\mathbf{u}}^{n-1}$,
2. set $\vec{\mathbf{v}} = [\mathbf{v}, 0]$ so that all terms involving ϕ drop out and we only need to use a fast Stokes solver to obtain $\mathbf{u}^{n+1}$;

Copyright © by SIAM. Unauthorized reproduction of this article is prohibited.

3. set $\vec{\mathbf{v}} = [0, \psi]$ so that all terms involving $\mathbf{u}$ drop out and we only need a fast Poisson solver to obtain ϕ^{n+1};
4. set $n = n + 1$ and return to step 1.

Note that steps 2 and 3 can be solved independently. Moreover, legacy codes can be used in each of those steps.

3. Unconditional and long-time stability. The goal of this section is to demonstrate the unconditional and long-time stability, with respect to the L^2-norm, of the two second-order schemes proposed in section 2. We first recall a few basic facts and some notation that are needed below.

Recall that the G-matrix associated with the classical (BDFZ) is given by

$$G = \begin{pmatrix} \frac{1}{2} & -1 \\ -1 & \frac{5}{2} \end{pmatrix}$$

with the associated G-norm given by $\|\mathbf{w}\|_G^2 = \big(\mathbf{w}, G\mathbf{w}\big)$ for all $\mathbf{w} \in (L^2(\Omega))^2$. The following identity is well known (see, e.g., [24]): for any $v_i \in L^2(\Omega)$, $i = 0, 1, 2$,

$$\left(\frac{3}{2}v_2 - 2v_1 + \frac{1}{2}v_0, v_2\right) = \frac{1}{2}\left(\|\mathbf{w}_1\|_G^2 - \|\mathbf{w}_0\|_G^2\right) + \frac{\|v_2 - 2v_1 + v_0\|^2}{4}, \tag{3.1}$$

where $\mathbf{w}_0 = [v_0, v_1]^T$ and $\mathbf{w}_1 = [v_1, v_2]^T$. We also apply the G matrix to functions belonging to $\mathbf{W}$: for any $\mathbf{w} \in \mathbf{W}^2$, define $|\mathbf{w}|_G^2 = \langle \mathbf{w}, G\mathbf{w}\rangle$. Then, for any $\vec{\mathbf{v}}_i \in W$, $i = 0, 1, 2$,

$$\left\langle\left\langle \frac{3}{2}\vec{\mathbf{v}}_2 - 2\vec{\mathbf{v}}_1 + \frac{1}{2}\vec{\mathbf{v}}_0, \vec{\mathbf{v}}_2 \right\rangle\right\rangle = \frac{1}{2}\left(|\mathbf{w}_1|_G^2 - |\mathbf{w}_0|_G^2\right) + \frac{\|\vec{\mathbf{v}}_2 - 2\vec{\mathbf{v}}_1 + \vec{\mathbf{v}}_0\|_S^2}{4},$$

where $\mathbf{w}_0 = [\vec{\mathbf{v}}^0, \vec{\mathbf{v}}^1]^T$ and $\mathbf{w}_1 = [\vec{\mathbf{v}}_1, \vec{\mathbf{v}}_2]^T$.

The G-norms are equivalent norms on $(L^2(\Omega))^2$ in the sense that there exists $C_l, C_u > 0$ such that

$$C_l\|\mathbf{w}\|_G^2 \le \|\mathbf{w}\|^2 \le C_u\|\mathbf{w}\|_G^2 \qquad \text{and} \qquad C_l\|\mathbf{w}\|_G^2 \le |\mathbf{w}|_G^2 \le C_u\|\mathbf{w}\|_G^2.$$

The following estimate follows from the basic inequalities. See [14].

LEMMA 3.1. *Let $a_\gamma(\cdot,\cdot)$ and $a_{st}(\cdot,\cdot)$ be defined as in* (2.4) *and* (2.8)*, respectively. Then, there exists a constant C_{ct} such that*

$$|a_{st}(\vec{\mathbf{u}}, \vec{\mathbf{v}})| + |a_\Gamma(\vec{\mathbf{u}}, \vec{\mathbf{v}})| \le C_{ct}\|\vec{\mathbf{u}}\|_\Gamma\|\vec{\mathbf{v}}\|_\Gamma \qquad \forall\, \vec{\mathbf{u}}, \vec{\mathbf{v}} \in \mathbf{W}.$$

For brevity, we introduce the *BDF difference operator* $Dv^{n+1} = \frac{3}{2}v^{n+1} - 2v^n + \frac{1}{2}v^{n-1}$ and the *central difference operator* $\delta v^{n+1} = v^{n+1} - 2v^n + v^{n-1}$.

3.1. Unconditional stability of the BDF2 and AMB2 schemes.

3.1.1. Unconditional stability of the BDF2 scheme.

THEOREM 3.2. *Let $T > 0$ be any fixed time. Then, the* BDF2 *scheme* (2.7) *is unconditionally stable on* $(0, T]$.

The proof relies on Lemma 3.1, the trace inequality, Young's inequality, basic energy estimates, and the utility of the following energy functional:

$$E_n = |\vec{\mathbf{w}}_n|_G^2 + \frac{C_a\Delta t}{(1 + (C_1 + C_2)\Delta t)}\|\nabla\vec{\mathbf{u}}^{n+1}\|^2 + \frac{C_a\Delta t}{3(1 + (C_1 + C_2)\Delta t)}\|\nabla\vec{\mathbf{u}}^n\|^2.$$

The interested reader is referred to [14] for the proof.

Copyright © by SIAM. Unauthorized reproduction of this article is prohibited.

Downloaded 03/17/23 to 131.151.26.204 . Redistribution subject to SIAM license or copyright; see https://epubs.siam.org/terms-privacy

Downloaded 03/17/23 to 131.151.26.204 . Redistribution subject to SIAM license or copyright; see https://epubs.siam.org/terms-privacy

3.1.2. Unconditional stability of the AMB2 scheme. We introduce the parameters

(3.2)
$$\alpha_1 = \Big|\frac{3}{2} - 2\alpha\Big|, \quad \alpha_2 = \Big|\alpha - \frac{1}{2}\Big|, \quad \beta_3 = \alpha_1 + \alpha_2, \quad \beta_1 = 2\alpha - \beta_3, \quad \beta_2 = \frac{1}{2}(\beta_1 + \beta_3).$$

THEOREM 3.3. *Let $T > 0$ be any fixed time and let $1/2 < \alpha < 1$. Then, the* AMB2 *scheme* (2.9) *is unconditionally stable in* $(0, T]$.

The proof can be found in [14]. Unconditional stability means that the numerical solution remains bounded (by a constant of the form of e^{cT}) on any finite time interval regardless of the size of the time-step.

3.2. Long-time stability of the BDF2 and AMB2 schemes.

3.2.1. Uniform in time estimates for the BDF2 scheme.

THEOREM 3.4. *Assume that $\vec{\mathbf{f}} \in L^\infty(L^2(\Omega))$ and that the time-step restriction* (3.8) *is satisfied. Then, the solution to the* BDF2 *scheme* (2.7) *is uniformly bounded for all time. Specifically, there exist $0 < \lambda_1 < 1$, $\lambda_2 < \infty$, and $E_0 \geq 0$ such that*

$$\|\vec{\mathbf{u}}^n\|^2 \leq C_u \lambda_1^n E_0 + \lambda_2.$$

Proof. Setting $\vec{\mathbf{v}} = \vec{\mathbf{u}}^{n+1} = \big(\mathbf{u}^{n+1}, \phi^{n+1}\big)$ in the BDF2 scheme (2.7), we have

$$\begin{aligned}&\frac{1}{\Delta t}\big\langle\big\langle D\vec{\mathbf{u}}^{n+1}, \vec{\mathbf{u}}^{n+1}\big\rangle\big\rangle + a(\vec{\mathbf{u}}^{n+1}, \vec{\mathbf{u}}^{n+1}) + a_{st}(\delta\vec{\mathbf{u}}^{n+1}, \vec{\mathbf{u}}^{n+1})\\ &\quad = \big\langle\big\langle\big\langle\vec{\mathbf{f}}^{n+1}, \vec{\mathbf{u}}^{n+1}\big\rangle\big\rangle\big\rangle - a_\Gamma(2\vec{\mathbf{u}}^n - \vec{\mathbf{u}}^{n-1}, \vec{\mathbf{u}}^{n+1}).\end{aligned}$$

From (3.1) and the skew-symmetry of $a_\Gamma(\cdot,\cdot)$, we obtain

$$\begin{aligned}&\frac{1}{2}|\vec{\mathbf{w}}_n|_G^2 - \frac{1}{2}|\vec{\mathbf{w}}_{n-1}|_G^2 + \frac{1}{4}\|\delta\vec{\mathbf{u}}^{n+1}\|_S^2 + \Delta t a(\vec{\mathbf{u}}^{n+1}, \vec{\mathbf{u}}^{n+1}) + \Delta t a_{st}(\vec{\mathbf{u}}^{n+1}, \vec{\mathbf{u}}^{n+1})\\ &\quad = \Delta t\Big(\big\langle\big\langle\big\langle\vec{\mathbf{f}}^{n+1}, \vec{\mathbf{u}}^{n+1}\big\rangle\big\rangle\big\rangle + \widetilde{a}_\Gamma(-2\vec{\mathbf{u}}^n + \vec{\mathbf{u}}^{n-1}, \vec{\mathbf{u}}^{n+1})\Big),\end{aligned} \tag{3.3}$$

Recall that $a_\Gamma(\vec{\mathbf{u}}^{n+1}, \vec{\mathbf{u}}^{n+1}) = 0$. Therefore, by Lemma 3.1,

$$\begin{aligned}&a_\Gamma(-2\vec{\mathbf{u}}^n + \vec{\mathbf{u}}^{n-1}, \vec{\mathbf{u}}^{n+1}) - a_{st}(\delta\vec{\mathbf{u}}^{n+1}, \vec{\mathbf{u}}^{n+1})\\ &\quad = \widetilde{a}_\Gamma(\delta\vec{\mathbf{u}}^{n+1}, \vec{\mathbf{u}}^{n+1}) \leq C_{ct}\left\|\delta\vec{\mathbf{u}}^{n+1}\right\|_\Gamma \left\|\vec{\mathbf{u}}^{n+1}\right\|_\Gamma.\end{aligned} \tag{3.4}$$

The trace and Poincaré inequalities imply

$$\begin{aligned}\left\|\delta\vec{\mathbf{u}}^{n+1}\right\|_\Gamma \left\|\vec{\mathbf{u}}^{n+1}\right\|_\Gamma &\leq C_{tr}^2 \|\delta\vec{\mathbf{u}}^{n+1}\|^{\frac{1}{2}} \|\nabla\delta\vec{\mathbf{u}}^{n+1}\|^{\frac{1}{2}} \|\nabla\vec{\mathbf{u}}^{n+1}\|\\ &\leq C_S^{\frac{1}{2}} C_{tr}^2 \|\delta\vec{\mathbf{u}}^{n+1}\|_S^{\frac{1}{2}} (\|\nabla\vec{\mathbf{u}}^{n+1}\|^{\frac{1}{2}} + \sqrt{2}\|\nabla\vec{\mathbf{u}}^n\|^{\frac{1}{2}} + \|\nabla\vec{\mathbf{u}}^{n-1}\|^{\frac{1}{2}}) \|\nabla\vec{\mathbf{u}}^{n+1}\|.\end{aligned} \tag{3.5}$$

The three terms on the right-hand side can be bounded using Young's inequalities:

$$\begin{aligned}\|\delta\vec{\mathbf{u}}^{n+1}\|_S^{\frac{1}{2}} \|\nabla\vec{\mathbf{u}}^{n+1}\|^{\frac{3}{2}} &\leq \frac{\varepsilon}{8}\|\nabla\vec{\mathbf{u}}^{n+1}\|^2 + \frac{54}{\varepsilon^3}\|\delta\vec{\mathbf{u}}^{n+1}\|_S^2,\\ \sqrt{2}\|\delta\vec{\mathbf{u}}^{n+1}\|_S^{\frac{1}{2}} \|\nabla\vec{\mathbf{u}}^n\|^{\frac{1}{2}} \|\nabla\vec{\mathbf{u}}^{n+1}\| &\leq \frac{\varepsilon}{8}\|\nabla\vec{\mathbf{u}}^{n+1}\|^2 + \frac{\varepsilon}{16}\|\nabla\vec{\mathbf{u}}^n\|^2 + \frac{64}{\varepsilon^3}\|\delta\vec{\mathbf{u}}^{n+1}\|_S^2,\\ \|\delta\vec{\mathbf{u}}^{n+1}\|_S^{\frac{1}{2}} \|\nabla\vec{\mathbf{u}}^{n-1}\|^{\frac{1}{2}} \|\nabla\vec{\mathbf{u}}^{n+1}\| &\leq \frac{\varepsilon}{8}\|\nabla\vec{\mathbf{u}}^{n+1}\|^2 + \frac{\varepsilon}{16}\|\nabla\vec{\mathbf{u}}^{n-1}\|^2 + \frac{16}{\varepsilon^3}\|\delta\vec{\mathbf{u}}^{n+1}\|_S^2.\end{aligned}$$

Copyright © by SIAM. Unauthorized reproduction of this article is prohibited.

Downloaded 03/17/23 to 131.151.26.204 . Redistribution subject to SIAM license or copyright; see https://epubs.siam.org/terms-privacy

Then, setting $\varepsilon = \varepsilon_0 = \frac{C_a}{C_S^{\frac{1}{2}} C_{ct} C_{tr}^2}$, we deduce from these three inequalities, (3.4), and (3.5) that

(3.6)
$$\widetilde{a}_\Gamma(\delta\vec{\mathbf{u}}^{n+1}, \vec{\mathbf{u}}^{n+1}) \le \frac{3C_a}{8} \left\|\nabla\vec{\mathbf{u}}^{n+1}\right\|^2 + \frac{C_a}{16} \|\nabla\vec{\mathbf{u}}^n\|^2 + \frac{C_a}{16} \left\|\nabla\vec{\mathbf{u}}^{n-1}\right\|^2 + \frac{134 {C_S}^2 C_{ct}^4 C_{tr}^8}{C_a^3} \left\|\delta\vec{\mathbf{u}}^{n+1}\right\|_S^2.$$

The forcing term can be bounded as

$$\left\langle\left\langle \vec{\mathbf{f}}^{n+1}, \mathbf{u}^{n+1}\right\rangle\right\rangle \le \frac{2C_P^2}{C_a}\|\vec{\mathbf{f}}^{n+1}\|^2 + \frac{C_a}{8C_P^2} \left\|\vec{\mathbf{u}}^{n+1}\right\|^2. \tag{3.7}$$

Combining (3.3) and (2.5) with (3.6) and (3.7), we obtain

$$|\vec{\mathbf{w}}_n|_G^2 + C_a\Delta t \left\|\nabla\vec{\mathbf{u}}^{n+1}\right\|^2 + \left[\frac{1}{2} - \frac{{C_S}^2 C_{ct}^4 C_{tr}^8}{C_a^3}\Delta t\right] \left\|\delta\vec{\mathbf{u}}^{n+1}\right\|_S^2 \le \frac{4C_P^2\Delta t}{C_a}\|\vec{\mathbf{f}}^{n+1}\|^2 + |\vec{\mathbf{w}}_{n-1}|_G^2 + \frac{C_a\Delta t}{8} \|\nabla\vec{\mathbf{u}}^n\|^2 + \frac{C_a\Delta t}{8} \left\|\nabla\vec{\mathbf{u}}^{n-1}\right\|^2.$$

Therefore, if the time-step restriction

$$\Delta t \le \frac{C_a^3}{536 {C_S}^2 C_{ct}^4 C_{tr}^8} \tag{3.8}$$

is satisfied, we deduce

$$|\vec{\mathbf{w}}_n|_G^2 + C_a\Delta t \left\|\nabla\vec{\mathbf{u}}^{n+1}\right\|^2 \le \frac{4C_P^2\Delta t}{C_a}\|\vec{\mathbf{f}}^{n+1}\|^2 + |\vec{\mathbf{w}}_{n-1}|_G^2 + \frac{C_a\Delta t}{8} \|\nabla\vec{\mathbf{u}}^n\|^2 + \frac{C_a\Delta t}{8} \left\|\nabla\vec{\mathbf{u}}^{n-1}\right\|^2,$$

where $C_a(\nu, gK_{min})$ and $C_S(gS)$ are defined one line below (2.5) and (2.6). Adding $\frac{3C_a\Delta t}{8} \|\nabla\vec{\mathbf{u}}^n\|^2$ to both sides of the above inequality, we obtain

$$|\vec{\mathbf{w}}_n|_G^2 + C_a\Delta t \left\|\nabla\vec{\mathbf{u}}^{n+1}\right\|^2 + \frac{3C_a\Delta t}{8} \|\nabla\vec{\mathbf{u}}^n\|^2 \le \frac{4C_P^2\Delta t}{C_a}\|\vec{\mathbf{f}}^{n+1}\|^2 + |\vec{\mathbf{w}}_{n-1}|_G^2 + \frac{C_a\Delta t}{2} \|\nabla\vec{\mathbf{u}}^n\|^2 + \frac{C_a\Delta t}{8} \left\|\nabla\vec{\mathbf{u}}^{n-1}\right\|^2,$$

which is equivalent to

$$E_n + \frac{C_a}{2}\Delta t \left\|\nabla\vec{\mathbf{u}}^{n+1}\right\|^2 + \frac{C_a}{4}\Delta t \|\nabla\vec{\mathbf{u}}^n\|^2 \le E_{n-1} + \frac{4C_P^2\Delta t}{C_a}\|\vec{\mathbf{f}}^{n+1}\|^2, \tag{3.9}$$

where $E_n = |\vec{\mathbf{w}}_n|_G^2 + \frac{C_a\Delta t}{2} \left\|\nabla\vec{\mathbf{u}}^{n+1}\right\|^2 + \frac{C_a\Delta t}{8} \|\nabla\vec{\mathbf{u}}^n\|^2$.

Utilizing the Poincaré inequality and the equivalence of the G-norm and the L^2-norm, we have

$$\frac{C_a}{2} \left\|\nabla\vec{\mathbf{u}}^{n+1}\right\|^2 + \frac{C_a}{4} \|\nabla\vec{\mathbf{u}}^n\|^2 \ge \frac{C_a}{4} \left\|\nabla\vec{\mathbf{u}}^{n+1}\right\|^2 + \frac{C_a}{8} \|\nabla\vec{\mathbf{u}}^n\|^2 + \frac{C_l^2 C_a}{8C_P^2}|\vec{\mathbf{w}}_n|_G^2.$$

Copyright © by SIAM. Unauthorized reproduction of this article is prohibited.

Downloaded 03/17/23 to 131.151.26.204 . Redistribution subject to SIAM license or copyright; see https://epubs.siam.org/terms-privacy

Therefore, setting $C_7 = \min\{\frac{C_l^2 C_a}{8C_P^2}, \frac{1}{2\Delta t}\}$, we have from (3.9) that

$$(1 + C_7\Delta t)E_n \le E_{n-1} + \frac{4C_P^2\Delta t}{C_a}\|\vec{\mathbf{f}}^{n+1}\|^2.$$

A simple induction argument leads to

$$E_n \le \Big(\frac{1}{1 + C_7\Delta t}\Big)^n E_0 + \frac{4C_P^2(1 + C_7\Delta t)}{C_a C_7}\max_i \|\vec{\mathbf{f}}^i\|^2.$$

Recall that $\|\vec{\mathbf{u}}^n\| \le C_u E_n$. Hence, the theorem is proved with $\lambda_1 = \frac{1}{1+C_7\Delta t}$ and $\lambda_2 = C_u\frac{4C_P^2(1+C_7\Delta t)}{C_a C_7}\max_i \|\vec{\mathbf{f}}^i\|^2$. ∎

The following corollary is used in the analysis of the fully discrete BDF2 scheme; see section 5.1.

COROLLARY 3.5. *In addition to the assumptions of Theorem* 3.4*, assume that the second time-step restriction* $\Delta t \le \frac{3C_a}{112C_s^2C_{ct}^2C_{tr}^4}$ *is satisfied. Then,*

$$\|\vec{\mathbf{u}}^n\|^2 \le C\lambda_1^{n-2}\big(\|\vec{\mathbf{u}}^0\|^2 + \|\vec{\mathbf{u}}^1\|^2 + \Delta t^2\|\nabla\vec{\mathbf{u}}^0\|^2 + \Delta t^2\|\nabla\vec{\mathbf{u}}^1\|^2\big) + C\lambda_2. \tag{3.10}$$

The interested reader is referred to [14] for the proof of this corollary.

3.2.2. Uniform in time estimates for the AMB2 scheme. We start with the following estimate.

LEMMA 3.6. *Let*

$$\mathcal{E}_\Gamma = -2a_\Gamma\left(\frac{3}{2}\vec{\mathbf{u}}^n - \frac{1}{2}\vec{\mathbf{u}}^{n-1}, \vec{\mathbf{u}}^{n+1}\right) - 2\alpha a_{st}\left(\delta\vec{\mathbf{u}}^{n+1}, \vec{\mathbf{u}}^{n+1}\right).$$

Then, with β_1 *and* β_2 *defined in* (3.2)*, we have the bound*

$$\begin{aligned}|\mathcal{E}_\Gamma| \le{}& \frac{4C_a(\beta_1 - \beta_2)}{9}\|\nabla\vec{\mathbf{u}}^{n+1}\|^2 + \frac{2C_a(\beta_1 - \beta_2)}{9}\|\nabla\vec{\mathbf{u}}^n\|^2\\ &+ \frac{C_a(\beta_1 - \beta_2)}{9}\|\nabla\vec{\mathbf{u}}^{n-1}\|^2 + (C_8 + C_9)\|\vec{\mathbf{u}}^{n+1} - \vec{\mathbf{u}}^n\|_S^2 + 2C_9\|\vec{\mathbf{u}}^n - \vec{\mathbf{u}}^{n-1}\|_S^2.\end{aligned} \tag{3.11}$$

THEOREM 3.7. *Assume that* $1/2 < \alpha < 1$, $\vec{\mathbf{f}} \in L^\infty(L^2(\Omega_f))$ *and that the time-step restriction* $\Delta t < \frac{1}{C_8+3C_9}$ *is satisfied. Then, the solution to the* AMB2 *scheme* (2.9) *is uniformly bounded for all time. Specifically, there exist* $0 < \lambda_3 < 1$, $\lambda_4 < \infty$, *and* $E_1 \ge 0$ *such that*

$$\|\vec{\mathbf{u}}^{n+1}\|^2 \le C_S\lambda_3^n E_1 + \lambda_4.$$

The interested reader may consult [14] for the proof.

Remark 1. Similarly to Corollary 3.5, in the error analysis, E_1 can be taken as $C(|\vec{\mathbf{w}}_0|_G + \Delta t^2(\|\nabla\vec{\mathbf{u}}_0\|^2 + \|\nabla\vec{\mathbf{u}}_1\|^1))$ in Theorem 3.7.

4. $H^1(\Omega)$ stability of the schemes. The purpose of this section is to prove uniform in time bounds for the solutions to the schemes (2.7) and (2.9) with respect to the $H^1(\Omega)$-norm. This additional estimate is needed for the estimation of finite element errors for the fluid velocity and hydraulic head with respect to the $H^1(\Omega)$-norm and for the pressure with respect to the $L^2(\Omega_f)$-norm; see section 5.1.

Copyright © by SIAM. Unauthorized reproduction of this article is prohibited.

Downloaded 03/17/23 to 131.151.26.204 . Redistribution subject to SIAM license or copyright; see https://epubs.siam.org/terms-privacy

4.1. Uniform in time $H^1(\Omega)$ bound of the BDF2 scheme. In this subsection, we assume that the time-step restriction (3.8) holds. We introduce the notation $\bar{\partial}\vec{\mathbf{u}}^{n+1} = \frac{1}{\Delta t}(\vec{\mathbf{u}}^{n+1} - \vec{\mathbf{u}}^n)$.

LEMMA 4.1. *The first-order discrete time derivative of the* BDF2 *scheme* (2.7) *is uniformly bounded in time. Specifically, we have*

$$\|\bar{\partial}\vec{\mathbf{u}}^{n+1}\|^2 \le C\lambda_1^n + C\max_i \|\bar{\partial}\vec{\mathbf{f}}^i\|^2, \tag{4.1}$$

where the positive parameter $\lambda_1 < 1$ is defined in Theorem 3.4.

The proof of this lemma is relatively straightforward. The proof also resembles the proof for Theorem 3.4 with $\vec{\mathbf{f}}$ replaced by $\bar{\partial}\vec{\mathbf{f}}$. The interested reader is referred to [14] for more details.

A direct consequence of Lemma 4.1 is the following result, once we realize that $\frac{1}{\Delta t}D\vec{\mathbf{u}}^{n+1} = \frac{3}{2}\bar{\partial}\vec{\mathbf{u}}^{n+1} - \frac{1}{2}\bar{\partial}\vec{\mathbf{u}}^n$ and $\frac{1}{\Delta t}\delta\vec{\mathbf{u}}^{n+1} = \bar{\partial}\vec{\mathbf{u}}^{n+1} - \bar{\partial}\vec{\mathbf{u}}^n$.

COROLLARY 4.2. *Let $\vec{\mathbf{u}}^n$ be the solution to the* BDF2 *scheme* (2.7). *Then,*

$$\left\|\frac{1}{\Delta t}D\vec{\mathbf{u}}^{n+1}\right\|^2 + \left\|\frac{1}{\Delta t}\delta\vec{\mathbf{u}}^{n+1}\right\|^2 \le C\lambda_1^n + C\max_i \|\bar{\partial}\vec{\mathbf{f}}^i\|^2. \tag{4.2}$$

The following technical lemma is useful in deriving the uniform in time $H^1(\Omega)$ bound.

LEMMA 4.3. *Let $\{a_n\}$ be a nonnegative sequence that satisfies*

$$a_{n+1} \le c_1\Delta t(a_n + a_{n-1}) + c_2\lambda^n + c_3 \quad \text{for } n = 1, 2, \ldots,$$

where c_i, $i = 1, 2, 3$, are positive numbers and $0 < \lambda < 1$. Moreover, if $\Delta t < \frac{2\lambda}{(1+\sqrt{5})c_1}$, then

$$a_{n+1} \le \frac{c_3}{1 - \frac{1+\sqrt{5}}{2}c_1\Delta t} + \lambda^n\left(\frac{c_2}{1 - \frac{1+\sqrt{5}}{2\lambda}c_1\Delta t} + a_1 + \frac{\sqrt{5}-1}{2}a_0\right). \tag{4.3}$$

The interested reader is referred to [14] for more details on the proof.

Remark 2. If $\Delta t < \frac{\lambda}{(1+\sqrt{5})c_1}$, then (4.3) implies

$$a_{n+1} \le 2c_3 + \lambda^n\left(2c_2 + a_1 + \frac{\sqrt{5}-1}{2}a_0\right).$$

THEOREM 4.4. *The* BDF2 *scheme* (2.7) *is asymptotically stable with respect to the $H^1(\Omega)$-norm in the sense that the $H^1(\Omega)$-norm of the solution is uniformly bounded in time.*

The proof relies on the previous lemma and corollary. The interested reader is referred to [14] for details.

4.2. Uniform in time $H^1(\Omega)$ bound for the AMB2 scheme. In this subsection, we assume that an appropriate time-step restriction holds. Utilizing the same arguments as for Lemma 4.1, we can deduce that the discrete time derivative of the solution of (2.9) is uniformly bounded in time.

THEOREM 4.5. *For the* AMB2 scheme, *we have*

$$\|\bar{\partial}\vec{\mathbf{u}}^{n+1}\|^2 \le C\lambda_3^{n-1} + C\max_i \|\bar{\partial}\vec{\mathbf{f}}^{i+\frac{1}{2}}\|^2,$$

where the positive parameter $\lambda_3 < 1$ is defined in Theorem 3.7. *Moreover, the* AMB2 *scheme is asymptotically stable with respect to the $H^1(\Omega)$-norm.*

The interested reader is referred to [14] for the proof.

Copyright © by SIAM. Unauthorized reproduction of this article is prohibited.

Downloaded 03/17/23 to 131.151.26.204 . Redistribution subject to SIAM license or copyright; see https://epubs.siam.org/terms-privacy

5. Error analysis. In this section, we study the convergence of the fully discrete BDF2 scheme, where spatial discretization is effected using finite element methods (FEMs). A similar study yielding similar results can be done for the AMB2 scheme; however, for brevity, we omit that study.

Let $\mathbf{H}_{f,h} \subset \mathbf{H}_f$, $H_{p,h} \subset H_p$, and $Q_h \subset Q$ denote conforming finite element spaces. Let $\mathbf{W}_h = \mathbf{H}_{f,h} \times H_{p,h}$. We assume that the mesh is regular and that the parameter h is a measure of the grid size. We use continuous piecewise polynomials of degrees k, k, and $k-1$ for the spaces $\mathbf{H}_{f,h}$, $H_{p,h}$, and Q_h, respectively. See [15] for details concerning such finite element discretizations. We also assume that the fluid velocity and pressure spaces $\mathbf{H}_{f,h}$ and Q_h satisfy the discrete inf-sup condition necessary for ensuring the stability of the finite element discretization; see [22].

DEFINITION 5.1. *The Stokes-Darcy projection $P_h : \mathbf{W} \times Q \to \mathbf{W}_h \times Q_h$ is defined as follows. For any $\vec{\mathbf{u}} \in \mathbf{W}$ and $p \in Q$, let $P_h\vec{\mathbf{u}} \in \mathbf{W}_h$ and $P_h p \in Q_h$ denote the finite element solution of*

$$\begin{aligned} a(P_h\vec{\mathbf{u}}, \vec{\mathbf{v}}_h) + b(\mathbf{v}_h, P_h p) + a_\Gamma(P_h\vec{\mathbf{u}}, \vec{\mathbf{v}}_h) &= a(\vec{\mathbf{u}}, \vec{\mathbf{v}}_h) + b(\mathbf{v}_h, p) + a_\Gamma(\vec{\mathbf{u}}, \vec{\mathbf{v}}_h), \\ b(P_h\mathbf{u}, q_h) &= b(\mathbf{u}, q_h) \end{aligned}$$

for all $\vec{\mathbf{v}}_h \in \mathbf{W}_h$ and $q_h \in Q_h$.

It is easy to see that for any $\vec{\mathbf{u}} \in \mathbf{W}$ and $p \in Q$, the exist unique $P_h\vec{\mathbf{u}} \in \mathbf{W}_h$ and $P_h p \in Q_h$. Moreover, if we assume that $\vec{\mathbf{u}} \in (H^{k+1}(\Omega_f))^d \times H^{k+1}(\Omega_p)$ and $p \in H^k(\Omega_f)$, then (see, e.g., [8]),

$$\|\vec{\mathbf{u}} - P_h\vec{\mathbf{u}}\| + h\|\nabla(\vec{\mathbf{u}} - P_h\vec{\mathbf{u}})\| \le h^{k+1}(\|\vec{\mathbf{u}}\|_{H^{k+1}} + \|p\|_{H^k}). \tag{5.1}$$

Remark 3. The estimate (5.1) and the optimal error estimates derived below assume that $\vec{\mathbf{u}} \in (H^{k+1})^d \times H^{k+1}(\Omega_p)$, which requires that the interface Γ be sufficiently smooth. In this case, the finite elements may need to be modified near the interface, e.g., by using isoparametric finite element approximations [15]. In any case, in this paper we assume that the optimal error order of convergence can be obtained for the steady-state Stokes–Darcy problems using the same grids and finite element spaces.

5.1. Error analysis of the BDF2-FEM scheme. The fully discrete BDF2-FEM scheme is defined as follows: for $n = 0, 1, 2 \ldots$, seek $\vec{\mathbf{u}}_h^{n+1} \in \mathbf{W}_h$ and $p_h^{n+1} \in Q_h$ such that

$$\begin{aligned} &\frac{1}{\Delta t}\big\langle\big\langle D\vec{\mathbf{u}}_h^{n+1}, \vec{\mathbf{v}}_h\big\rangle\big\rangle + a(\vec{\mathbf{u}}_h^{n+1}, \vec{\mathbf{v}}_h) + b(\mathbf{v}_h, p_h^{n+1}) + a_{st}(\vec{\mathbf{u}}_h^{n+1}, \vec{\mathbf{v}}_h) \\ &\qquad = \big\langle\big\langle\big\langle \vec{\mathbf{f}}^{n+1}, \vec{\mathbf{v}}_h\big\rangle\big\rangle\big\rangle - a_\Gamma(2\vec{\mathbf{u}}_h^n - \vec{\mathbf{u}}_h^{n-1}, \vec{\mathbf{v}}_h) + a_{st}(2\vec{\mathbf{u}}_h^n - \vec{\mathbf{u}}_h^{n-1}, \vec{\mathbf{v}}_h), \\ &b(\mathbf{u}_h^{n+1}, q_h) = 0, \end{aligned} \tag{5.2}$$

are satisfied for all $\vec{\mathbf{v}}_h \in \mathbf{W}_h$ and $q_h \in Q_h$. Note that for all $\vec{\mathbf{v}}_h \in \mathbf{W}_h$ and $q_h \in Q_h$, the exact solution satisfies

$$\big\langle\big\langle \vec{\mathbf{u}}_t, \vec{\mathbf{v}}_h\big\rangle\big\rangle + a(\vec{\mathbf{u}}, \vec{\mathbf{v}}_h) + a_\Gamma(\vec{\mathbf{u}}, \vec{\mathbf{v}}_h) + b(\mathbf{v}_h, p) = \big\langle\big\langle\big\langle \vec{\mathbf{f}}, \vec{\mathbf{v}}_h\big\rangle\big\rangle\big\rangle, \quad b(\mathbf{u}, q_h) = 0. \tag{5.3}$$

THEOREM 5.2. *Assume that the solution of the Stokes–Darcy problem* (2.1) *is sufficiently regular in the sense that*

$$\vec{\mathbf{u}} \in H^3(0, T; H^1) \cap H^2(0, T; H^{k+1}),$$

Copyright © by SIAM. Unauthorized reproduction of this article is prohibited.

that the time-step restrictions (3.8) *and* $\Delta t \le \frac{3C_a}{112C_s^2C_{ct}^2C_{tr}^4}$ *are satisfied, and that the finite element spaces are chosen so that the projection error bound* (5.1) *holds. Then, the solution of the fully discrete* BDF2 *scheme* (5.2) *satisfies the error estimate*

$$\|\vec{\mathbf{u}}(t)-\vec{\mathbf{u}}_h^n\|^2 \le \|P_h\vec{\mathbf{u}}(t_0)-\vec{\mathbf{u}}_h^0\|^2+\|P_h\vec{\mathbf{u}}(t_1)-\vec{\mathbf{u}}_h^1\|^2+C\Delta t(\|\nabla(P_h\vec{\mathbf{u}}(t_0)-\vec{\mathbf{u}}_h^0)\|^2 + \|\nabla(P_h\vec{\mathbf{u}}(t_1)-\vec{\mathbf{u}}_h^1)\|^2)+C(\Delta t^4+h^{2(k+1)}).$$

Moreover, if the solution of the Stokes–Darcy problem (2.1) *is long-time regular in the sense that*

$$\vec{\mathbf{u}} \in W^{3,\infty}(0,\infty;H^1)\cap W^{2,\infty}(0,\infty;H^{k+1}),$$

then there exists a constant C_a *and a generic constant* C *independent of* $\Delta t, h,$ *or* n *such that the solution of the* BDF2 *scheme* (5.2) *satisfies the* uniform in time error estimates

$$\begin{aligned}\|\vec{\mathbf{u}}(t_n)-\vec{\mathbf{u}}_h^n\|^2 &\le C\lambda_1^{n-2}(\|P_h\vec{\mathbf{u}}(t_0)-\vec{\mathbf{u}}_h^0\|^2+\|P_h\vec{\mathbf{u}}(t_1)-\vec{\mathbf{u}}_h^1\|^2)\\ &\quad + C\Delta t^2\lambda_1^{n-2}(\|\nabla(P_h\vec{\mathbf{u}}(t_0)-\vec{\mathbf{u}}_h^0)\|^2+\|\nabla(P_h\vec{\mathbf{u}}(t_1)-\vec{\mathbf{u}}_h^1)\|^2)\\ &\quad + C(\Delta t^4+h^{2(k+1)}) \quad \forall\, n\end{aligned} \tag{5.4}$$

and

$$\begin{aligned}&\|\nabla(\vec{\mathbf{u}}(t_{n+1})-\vec{\mathbf{u}}_h^{n+1})\|^2+\|p(t_{n+1})-p_h^{n+1}\|^2\\ &\quad\le C\lambda_1^{n-2}(\|\bar\partial P_h\vec{\mathbf{u}}(t_1)-\bar\partial\vec{\mathbf{u}}_h^1\|^2+\|\bar\partial P_h\vec{\mathbf{u}}(t_2)-\bar\partial\vec{\mathbf{u}}_h^2\|^2)\\ &\qquad + C\Delta t^2\lambda_1^{n-2}(\|\nabla(\bar\partial P_h\vec{\mathbf{u}}(t_1)-\bar\partial\vec{\mathbf{u}}_h^1)\|^2+\|\nabla(\bar\partial P_h\vec{\mathbf{u}}(t_2)-\bar\partial\vec{\mathbf{u}}_h^2)\|^2)\\ &\qquad + C(\Delta t^2+h^{2k}) \quad \forall\, n\end{aligned}$$

provided that $\Delta t \le C_a$.

Proof. Let $\vec{\mathbf{e}}^n=\vec{\mathbf{u}}(t_n)-\vec{\mathbf{u}}_h^n$ denote the error at the time $t=t_n$. Then, from (5.2) and (5.3), we have

$$\begin{aligned}&\frac{1}{\Delta t}\langle\langle D\vec{\mathbf{e}}^{n+1},\vec{\mathbf{v}}_h\rangle\rangle+a(\vec{\mathbf{e}}^{n+1},\vec{\mathbf{v}}_h)+b(\mathbf{v}_h,p(t_{n+1})-p_h^{n+1})+a_\Gamma(\vec{\mathbf{e}}^{n+1},\vec{\mathbf{v}}_h)\\ &\qquad -\widetilde{a}_\Gamma(\delta\vec{\mathbf{e}}^{n+1},\vec{\mathbf{v}}_h)=\langle\langle\omega_1^{n+1},\vec{\mathbf{v}}_h\rangle\rangle-\widetilde{a}_\Gamma(\delta\vec{\mathbf{u}}(t_{n+1}),\vec{\mathbf{v}}_h),\\ &\qquad\qquad b(\mathbf{e}^{n+1},q_h)=0,\end{aligned} \tag{5.5}$$

where $\boldsymbol{\omega}_1^{n+1}=-\vec{\mathbf{u}}_t(t_{n+1})+\frac{1}{\Delta t}D\vec{\mathbf{u}}(t_{n+1})$. Let $\vec{\boldsymbol{\rho}}^n=\vec{\mathbf{u}}(t_n)-P_h\vec{\mathbf{u}}(t_n)$ and $\vec{\boldsymbol{\theta}}^n=P_h\vec{\mathbf{u}}(t_n)-\vec{\mathbf{u}}_h^n$. Then, $\vec{\boldsymbol{\theta}}^n\in\mathbf{W}_h$ and is discretely divergence free, i.e.,

$$b(\boldsymbol{\theta}^n,q_h)=0 \quad \forall\, q_h\in Q_h. \tag{5.6}$$

Because $\vec{\mathbf{e}}^n=\vec{\boldsymbol{\theta}}^n+\vec{\boldsymbol{\rho}}^n$, the error equation (5.5) can be recast as

$$\begin{aligned}&\frac{1}{\Delta t}\langle\langle D\vec{\boldsymbol{\theta}}^{n+1},\vec{\mathbf{v}}_h\rangle\rangle+a(\vec{\boldsymbol{\theta}}^{n+1},\vec{\mathbf{v}}_h)+a_\Gamma(\vec{\boldsymbol{\theta}}^{n+1},\vec{\mathbf{v}}_h)-\widetilde{a}_\Gamma(\delta\vec{\boldsymbol{\theta}}^{n+1},\vec{\mathbf{v}}_h)\\ &\quad=\langle\langle\boldsymbol{\omega}_1^{n+1},\vec{\mathbf{v}}_h\rangle\rangle-\widetilde{a}_\Gamma(\delta\vec{\mathbf{u}}(t_{n+1}),\vec{\mathbf{v}}_h)-b(\mathbf{v}_h,p(t_{n+1})-p_h^{n+1})\\ &\qquad-\frac{1}{\Delta t}\langle\langle D\vec{\boldsymbol{\rho}}^{n+1},\vec{\mathbf{v}}_h\rangle\rangle-a(\vec{\boldsymbol{\rho}}^{n+1},\vec{\mathbf{v}}_h)-a_\Gamma(\vec{\boldsymbol{\rho}}^{n+1},\vec{\mathbf{v}}_h)+\widetilde{a}_\Gamma(\delta\vec{\boldsymbol{\rho}}^{n+1},\vec{\mathbf{v}}_h)\\ &\quad=\langle\langle\boldsymbol{\omega}_1^{n+1},\vec{\mathbf{v}}_h\rangle\rangle-\widetilde{a}_\Gamma(\delta\vec{\mathbf{u}}(t_{n+1}),\vec{\mathbf{v}}_h)-b(\mathbf{v}_h,P_hp(t_{n+1})-p_h^{n+1})\\ &\qquad-\frac{1}{\Delta t}\langle\langle D\vec{\boldsymbol{\rho}}^{n+1},\vec{\mathbf{v}}_h\rangle\rangle+\widetilde{a}_\Gamma(\delta\vec{\boldsymbol{\rho}}^{n+1},\vec{\mathbf{v}}_h).\end{aligned}$$

Copyright © by SIAM. Unauthorized reproduction of this article is prohibited.

Downloaded 03/17/23 to 131.151.26.204 . Redistribution subject to SIAM license or copyright; see https://epubs.siam.org/terms-privacy

Downloaded 03/17/23 to 131.151.26.204 . Redistribution subject to SIAM license or copyright; see https://epubs.siam.org/terms-privacy

Setting $\vec{\mathbf{v}}_h = \vec{\boldsymbol{\theta}}^{n+1}$, noting that $a_\Gamma(\vec{\boldsymbol{\theta}}^{n+1}, \vec{\boldsymbol{\theta}}^{n+1}) = 0$, and using (5.6) results in

$$\begin{aligned}\frac{1}{\Delta t}\langle\langle D\vec{\boldsymbol{\theta}}^{n+1}, \vec{\boldsymbol{\theta}}^{n+1}\rangle\rangle + a(\vec{\boldsymbol{\theta}}^{n+1}, \vec{\boldsymbol{\theta}}^{n+1}) - \widetilde{a}_\Gamma(\delta\vec{\boldsymbol{\theta}}^{n+1}, \vec{\boldsymbol{\theta}}^{n+1}) = \langle\langle \boldsymbol{\omega}_1^{n+1}, \vec{\boldsymbol{\theta}}^{n+1}\rangle\rangle \\ - \widetilde{a}_\Gamma(\delta\vec{\mathbf{u}}(t_{n+1}), \vec{\boldsymbol{\theta}}^{n+1}) - \frac{1}{\Delta t}\langle\langle D\vec{\boldsymbol{\rho}}^{n+1}, \vec{\boldsymbol{\theta}}^{n+1}\rangle\rangle + \widetilde{a}_\Gamma(\delta\vec{\boldsymbol{\rho}}^{n+1}, \vec{\boldsymbol{\theta}}^{n+1}).\end{aligned} \tag{5.7}$$

Letting $\vec{\mathbf{w}}_n = [\vec{\boldsymbol{\theta}}^{n+1}, \vec{\boldsymbol{\theta}}^{n}]^T$ and $E_n = |\vec{\mathbf{w}}_n|_G^2 + \frac{C_a\Delta t}{2}\|\nabla\vec{\boldsymbol{\theta}}^{n+1}\|^2 + \frac{C_a\Delta t}{8}\|\nabla\vec{\boldsymbol{\theta}}^{n}\|^2$ and following the lines of the proof of Theorem 3.4, we have

$$\begin{aligned}E_n + \frac{C_a}{2}\Delta t\left\|\nabla\vec{\boldsymbol{\theta}}^{n+1}\right\|^2 + \frac{C_a}{4}\Delta t\left\|\nabla\vec{\boldsymbol{\theta}}^{n}\right\|^2 \le E_{n-1} \\ + C\Delta t\left(\|\boldsymbol{\omega}_1^{n+1}\|^2 + \|\nabla\delta\vec{\mathbf{u}}(t_{n+1})\|^2 + \left\|\frac{1}{\Delta t}D\vec{\boldsymbol{\rho}}^{n+1}\right\|^2 + \|\nabla\delta\vec{\boldsymbol{\rho}}^{n+1}\|^2\right).\end{aligned} \tag{5.8}$$

By Taylor's theorem with the integral form of the remainder, we have

$$\|\boldsymbol{\omega}_1^{n+1}\|^2 \le C\Delta t^3\int_{t_{n-1}}^{t_{n+1}}\|\vec{\mathbf{u}}_{ttt}\|^2dt \le C\Delta t^4\|\vec{\mathbf{u}}_{ttt}\|^2_{L^\infty(0,t_{n+1})} \tag{5.9}$$

and

$$\|\nabla\delta\vec{\mathbf{u}}(t_{n+1})\|^2 \le C\Delta t^3\int_{t_{n-1}}^{t_{n+1}}\|\nabla\vec{\mathbf{u}}_{ttt}\|^2dt \le C\Delta t^4\|\nabla\vec{\mathbf{u}}_{ttt}\|^2_{L^\infty(0,t_{n+1})}. \tag{5.10}$$

Moreover, using (5.1), we have

$$\begin{aligned}\left\|\frac{1}{\Delta t}D\vec{\boldsymbol{\rho}}^{n+1}\right\|^2 &\le Ch^{2(k+1)}\left\|\frac{1}{\Delta t}D\vec{\mathbf{u}}(t_{n+1})\right\|^2_{H^{k+1}} \\ &\le C\frac{h^{2(k+1)}}{\Delta t}\int_{t_{n-1}}^{t_{n+1}}\|\vec{\mathbf{u}}_t\|^2_{H^{k+1}}dt \le Ch^{2(k+1)}\|\vec{\mathbf{u}}_t\|^2_{L^\infty(0,t_{n+1};H^{k+1})}\end{aligned} \tag{5.11}$$

and

$$\begin{aligned}\|\nabla\delta\vec{\boldsymbol{\rho}}^{n+1}\|^2 \le Ch^{2k}\|\delta\vec{\mathbf{u}}(t_{n+1})\|^2_{H^{k+1}} &\le Ch^{2k}\Delta t^3\int_{t_{n-1}}^{t_{n+1}}\|\vec{\mathbf{u}}_{tt}\|^2_{H^{k+1}}dt \\ &\le Ch^{2k}\Delta t^4\|\vec{\mathbf{u}}_{tt}\|^2_{L^\infty(0,t_{n+1};H^{k+1})}.\end{aligned} \tag{5.12}$$

Combining (5.8)–(5.12), we have

$$\begin{aligned}E_n + \frac{C_a}{2}\Delta t\sum_{i=1}^{n+1}\left\|\nabla\vec{\theta}^i\right\|^2 \le E_0 + C\Bigg(\Delta t^4\int_0^{t_{n+1}}(\|\vec{\mathbf{u}}_{ttt}\|^2 + \|\nabla\vec{\mathbf{u}}_{ttt}\|^2)dt \\ + h^{2(k+1)}\int_0^{t_{n+1}}\|\vec{\mathbf{u}}_t\|^2_{H^{k+1}}dt + h^{2k}\Delta t^4\int_0^{t_{n+1}}\|\vec{\mathbf{u}}_{tt}\|^2_{H^{k+1}}dt\Bigg).\end{aligned} \tag{5.13}$$

The desired finite time error estimate follows from this and the assumed bound on the projection error $\vec{\boldsymbol{\rho}}^n$.

For the uniform in time $L^2(\Omega)$ bound, we again use (5.8)–(5.12) to obtain

$$\begin{aligned}&E_n + \frac{C_a}{2}\Delta t\left\|\nabla\vec{\boldsymbol{\theta}}^{n+1}\right\|^2 + \frac{C_a}{4}\Delta t\left\|\nabla\vec{\boldsymbol{\theta}}^{n}\right\|^2 \\ &\quad\le E_{n-1} + C\Delta t\Big(\Delta t^4\|\vec{\mathbf{u}}_{ttt}\|^2_{L^\infty(0,\infty)} + \Delta t^4\|\nabla\vec{\mathbf{u}}_{ttt}\|^2_{L^\infty(0,\infty)} \\ &\qquad + h^{2(k+1)}\|\vec{\mathbf{u}}_t\|^2_{L^\infty(0,\infty;H^{k+1})} + h^{2k}\Delta t^4\|\vec{\mathbf{u}}_{tt}\|^2_{L^\infty(0,\infty;H^{k+1})}\Big) \\ &\quad\le E_{n-1} + C\Delta t(\Delta t^4 + h^{2(k+1)}).\end{aligned} \tag{5.14}$$

Copyright © by SIAM. Unauthorized reproduction of this article is prohibited.

Downloaded 03/17/23 to 131.151.26.204 . Redistribution subject to SIAM license or copyright; see https://epubs.siam.org/terms-privacy

Using the Poincaré inequality and the definition of the G-norm, we have

$$\frac{C_a}{2}\Delta t\left\|\nabla\vec{\boldsymbol{\theta}}^{n+1}\right\|^2+\frac{C_a}{4}\Delta t\left\|\nabla\vec{\boldsymbol{\theta}}^{n}\right\|^2 \geq \frac{C_a}{4}\Delta t\left\|\nabla\vec{\boldsymbol{\theta}}^{n+1}\right\|^2+\frac{C_a}{8}\Delta t\left\|\nabla\vec{\boldsymbol{\theta}}^{n}\right\|^2+\frac{C_l^2C_a}{8C_P^2}|\vec{\mathbf{w}}_n|_G^2.$$

Then, with C_7 defined as in Theorem 3.4, we have from (5.14),

$$(1+C_7\Delta t)E_n\leq E_{n-1}+C\Delta t(\Delta t^4+h^{2(k+1)}).$$

A simple induction argument then leads to

$$\begin{aligned}E_n&\leq\Big(\frac{1}{1+C_7\Delta t}\Big)^{n-2}E_2+C(\Delta t^4+h^{2(k+1)})\\&\leq C\lambda_1^{n-2}(\|\vec{\boldsymbol{\theta}}^1\|^2+\|\vec{\boldsymbol{\theta}}^0\|^2)+C\lambda_1^n\Delta t(\|\nabla\vec{\boldsymbol{\theta}}^1\|^2+\|\nabla\vec{\boldsymbol{\theta}}^0\|^2)+C(\Delta t^4+h^{2(k+1)}),\end{aligned}$$

where λ_1 is defined as in Theorem 3.4. The bound (5.4) then follows from Corollary 3.4.

The uniform in time $H^1(\Omega)$-norm error estimate on the velocity and the $L^2(\Omega)$ error estimate on the pressure can be derived as well after we combine the technique used above with techniques from section 4. Indeed, from (5.9) and (5.10) and using the triangle inequality, we have

$$\|\bar\partial\boldsymbol{\omega}_1^{n+1}\|^2\leq C\Delta t\int_{t_{n-2}}^{t_{n+1}}\|\vec{\mathbf{u}}_{ttt}\|^2dt\leq C\Delta t^2\|\vec{\mathbf{u}}_{ttt}\|^2_{L^\infty(0,t_{n+1})}\tag{5.15}$$

and

$$\|\nabla\bar\partial\delta\vec{\mathbf{u}}(t_{n+1})\|^2\leq C\Delta t\int_{t_{n-2}}^{t_{n+1}}\|\nabla\vec{\mathbf{u}}_{ttt}\|^2dt\leq C\Delta t^2\|\nabla\vec{\mathbf{u}}_{ttt}\|^2_{L^\infty(0,t_{n+1})}.\tag{5.16}$$

Moreover, by the definitions of P_h, $\bar\partial$, and D,

(5.17)
$$\begin{aligned}\left\|\frac{1}{\Delta t}\bar\partial D\vec{\boldsymbol{\rho}}^{n+1}\right\|^2&\leq Ch^{2(k+1)}\left\|\frac{1}{\Delta t}\bar\partial D\vec{\mathbf{u}}(t_{n+1})\right\|^2_{H^{k+1}}\\&\leq C\frac{h^{2(k+1)}}{\Delta t}\int_{t_{n-2}}^{t_{n+1}}\|\vec{\mathbf{u}}_{tt}\|^2_{H^{k+1}}dt\leq Ch^{2(k+1)}\|\vec{\mathbf{u}}_{tt}\|^2_{L^\infty(0,t_{n+1};H^{k+1})},\end{aligned}$$

and by the triangle inequality and (5.12),

$$\|\nabla\bar\partial\delta\vec{\boldsymbol{\rho}}^{n+1}\|^2\leq Ch^{2k}\Delta t^2\|\vec{\mathbf{u}}_{tt}\|^2_{L^\infty(0,t_{n+1};H^{k+1})}.\tag{5.18}$$

We combine (5.15)–(5.18) with the stability proof of Lemma 4.1 with a small modification for the initial steps; see Corollary 3.5. As a result, we obtain

$$\begin{aligned}\|\bar\partial\vec{\boldsymbol{\theta}}^{n+1}\|^2&\leq C\lambda_1^{n-2}(\|\bar\partial\vec{\boldsymbol{\theta}}^1\|^2+\|\bar\partial\vec{\boldsymbol{\theta}}^2\|^2)\\&\quad+C\Delta t^2\lambda_1^{n-2}(\|\nabla\bar\partial P_h\vec{\boldsymbol{\theta}}^1\|^2+\|\nabla\bar\partial P_h\vec{\boldsymbol{\theta}}^2\|^2)+C(\Delta t^2+h^{2(k+1)}).\end{aligned}\tag{5.19}$$

Note that

$$\left\|\frac{\delta\vec{\mathbf{u}}(t_i)}{\Delta t}\right\|^2\leq C\Delta t^2\|\vec{\mathbf{u}}_{tt}\|^2_{L^\infty(0,t_i)},\quad\left\|\frac{\delta\boldsymbol{\rho}^i}{\Delta t}\right\|^2\leq C\Delta t^2h^{2(k+1)}\|\vec{\mathbf{u}}_{tt}\|^2_{L^\infty(0,t_i;H^{k+1})}.\tag{5.20}$$

Combining (5.19) and (5.20) with (5.9) and (5.11) and following the proof of Theorem 4.4, we have from (5.7)

Copyright © by SIAM. Unauthorized reproduction of this article is prohibited.

$$\|\nabla\vec{\boldsymbol{\theta}}^{n+1}\|^2 \le C\lambda_1^{n-2}(\|\bar{\partial}\vec{\boldsymbol{\theta}}^1\|^2 + \|\bar{\partial}\vec{\boldsymbol{\theta}}^2\|^2 + \Delta t^2(\|\nabla\bar{\partial}P_h\vec{\boldsymbol{\theta}}^1\|^2 + \|\nabla\bar{\partial}P_h\vec{\boldsymbol{\theta}}^2\|^2)) + C(\Delta t^2 + h^{2(k+1)}).$$

After adding the estimate of $\|\nabla\vec{\boldsymbol{\rho}}^{n+1}\|$ (see (5.1)), we obtain the bound for $\|\nabla(\vec{\mathbf{u}}(t_{n+1}) - \vec{\mathbf{u}}_h^{n+1})\|^2$. ∎

Remark 4. The uniform in time estimates given above imply that the method can be used to obtain an approximate solution of the steady-state equations in case the forcing term is time independent. This follows because the truncation errors listed in (5.8)–(5.12) vanish for the time-independent problem. Consequently, we have

$$\|\vec{\mathbf{u}}_h^n - \vec{\mathbf{u}}^n\|^2 \le C\lambda_1^n(\|\vec{\mathbf{u}}_h^0 - \vec{\mathbf{u}}^0\|^2 + \Delta t\|\nabla(\vec{\mathbf{u}}_h^0 - \vec{\mathbf{u}}^0)\|^2)$$

for the steady-state problem.

In the steady-state case, the methods we study can be viewed as a domain decomposition method with the discrete time n playing the role of an iteration number; see [13] for a related scheme. The current scheme also enjoys an exponential rate of convergence, as does the iterative scheme proposed in [13].

Remark 5. Note that the uniform in time error estimate for the velocity with respect to the $H^1(\Omega)$-norm and the uniform error estimate for the pressure are not second-order in time. We do not know if this is an artifact of our approach. However, our numerical experiments in the next section suggest that the long-time convergence rate for the pressure approximation may very well be first-order as the analysis suggests.

6. Numerical results. Using three numerical examples, we now illustrate the theoretical results of the previous section.

As was done in previous work [13, 37], we set $\Omega_f = (0,1)\times(1,2)$ and $\Omega_p = (0,1)\times(0,1)$, with Ω_f and Ω_p separated by the interface $\Gamma = (0,1)\times\{1\}$. We choose the standard continuous piecewise-quadratic finite element space, defined with respect to the matrix domain Ω_p, for approximating the hydraulic head ϕ. We also choose the Hood–Taylor element pair, defined with respect to the conduit domain Ω_f, i.e., continuous piecewise-quadratic and continuous piecewise-linear finite element spaces for the fluid velocity and pressure approximations, respectively. Uniform triangular meshes are created by first dividing the rectangular domains Ω_p and Ω_f into identical small squares and then dividing each square into two triangles. For illustrating the short-time properties of our schemes, we set the final time to $T = 1$; for illustrating the long-time behavior, we set $T = 100$.

We use two examples with exact solutions. Example 1 is taken from [37], and Example 2 is a slight modification of an example in [8]. To illustrate the accuracy of our schemes, we assume that the error is of the order $O(h^{\theta_1} + \Delta t^{\theta_2})$. We set $\Delta t = h^\theta$ and quantify the numerically estimated order of convergence $r_\theta = \min(\theta_1, \theta\theta_2)$ with respect to h by calculating $r_\theta \approx \log_2 \frac{\|u_{2h,\theta} - u_{exact}\|_{l^2}}{\|u_{h,\theta} - u_{exact}\|_{l^2}}$. Here, we use the discrete L^2-norm of nodal values to measure errors.

Example 1. We set the exact solution to [37]

$$\mathbf{u}_f(\mathbf{x},t) = \Big([x^2(y-1)^2 + y]\cos t,\ \Big[-\frac{2}{3}x(y-1)^3 + 2 - \pi\sin(\pi x)\Big]\cos t\Big),$$
$$p_f(\mathbf{x},t) = [2 - \pi\sin(\pi x)]\sin\Big(\frac{\pi}{2}y\Big)\cos t,$$
$$\phi(\mathbf{x},t) = [2 - \pi\sin(\pi x)][1 - y - \cos(\pi y)]\cos t.$$

Copyright © by SIAM. Unauthorized reproduction of this article is prohibited.

Downloaded 03/17/23 to 131.151.26.204 . Redistribution subject to SIAM license or copyright; see https://epubs.siam.org/terms-privacy

Downloaded 03/17/23 to 131.151.26.204 . Redistribution subject to SIAM license or copyright; see https://epubs.siam.org/terms-privacy

The right-side data in the partial differential equations, initial conditions, and boundary conditions are then chosen correspondingly. As done in [37], we set the parameters $\gamma_p = \gamma_f = g = S = \nu = \alpha_{BJSJ} = 1$ and $\mathbb{K} = \mathbb{I}$; also, we set $\alpha = 0.8$ for the AMB2 scheme.

For Table 6.1, we set $\Delta t = h$ and present results for several values of h; the results illustrate the second-order in time accuracy for ϕ, $\mathbf{u}_f$, and p_f. We also notice that BDF2 has a significantly smaller error than AMB2, illustrating the advantage of the former over the latter scheme, at least for this example. For Tables 6.2 and 6.3, Δt is chosen to be a power of h to illustrate the spatial convergence rates. The results in those tables indicate that the spatial accuracy seems higher than the third-order suggested by our analysis. The extra half-order of accuracy may be attributed to superconvergence or superapproximation behaviors; see [12] for a study of this phenomenon for the steady-state case.

Example 2. To illustrate the long-time behavior of our schemes, we use the following exact solution that is a slight modification of an example in [8]:

$$\begin{aligned}
\mathbf{u}_f(\mathbf{x},t) &= \Big([x^2y^2 + e^{-y}], \Big[-\frac{2}{3}xy^3 + [2 - \pi\sin(\pi x)]\Big]\Big)[2 + \cos(2\pi t)] \\
p_f(\mathbf{x},t) &= -[2 - \pi\sin(\pi x)]\cos(2\pi y)[2 + \cos(2\pi t)] \\
\phi(\mathbf{x},t) &= [2 - \pi\sin(\pi x)][-y + \cos(\pi(1-y))][2 + \cos(2\pi t)].
\end{aligned}$$

TABLE 6.1
Relative error and order of accuracy with respect to the spatial grid size h for Example 1 at $t = 1$ and with $\Delta t = h$.

	e_ϕ		$e_{\mathbf{u}}$		e_p	
h	BDF2	AMB2	BDF2	AMB2	BDF2	AMB2
1/16	5.76e-005	3.43e-003	8.26e-005	1.11e-004	1.15e-002	4.11e-002
1/32	9.53e-006	8.76e-004	1.98e-005	2.74e-005	3.02e-003	1.07e-002
1/64	2.35e-006	2.21e-004	4.85e-006	6.79e-006	7.73e-004	2.71e-003
1/128	6.00e-007	5.55e-005	1.20e-006	1.69e-006	1.96e-004	6.85e-004
r_{avg}	2.20	1.98	2.04	2.01	1.97	1.97

TABLE 6.2
Same information as in Table 6.1 but for $\Delta t = h^{3.5/2}$.

	e_ϕ		$e_{\mathbf{u}}$		e_p	
h	BDF2	AMB2	BDF2	AMB2	BDF2	AMB2
1/8	6.16e-004	6.83e-004	8.14e-005	8.37e-005	2.81e-002	3.04e-002
1/16	5.39e-005	6.46e-005	7.67e-006	7.86e-006	7.71e-003	7.93e-003
1/32	4.70e-006	6.01e-006	6.99e-007	7.16e-007	2.03e-003	2.05e-003
1/64	4.13e-007	5.51e-007	6.26e-008	6.41e-008	5.22e-004	5.24e-004
r_{avg}	3.51	3.43	3.45	3.45	1.92	1.95

TABLE 6.3
Same information as in Table 6.1 but for $\Delta t = h^2$.

	e_ϕ		$e_{\mathbf{u}}$		e_p	
h	BDF2	AMB2	BDF2	AMB2	BDF2	AMB2
1/8	6.17e-004	5.82e-004	8.11e-005	8.17e-005	2.78e-002	2.85e-002
1/16	5.40e-005	5.21e-005	7.66e-006	7.69e-006	7.65e-003	7.73e-003
1/32	4.71e-006	4.62e-006	6.99e-007	7.01e-007	2.04e-003	2.03e-003
1/64	4.13e-007	4.09e-007	6.26e-008	6.28e-008	5.22e-004	5.22e-004
r_{avg}	3.52	3.49	3.45	3.45	1.91	1.92

Copyright © by SIAM. Unauthorized reproduction of this article is prohibited.

In this long-time numerical experiment, we set the terminal time $T = 100$ and $h = 1/64$. We choose $\Delta t = \frac{1}{128}, \frac{1}{256}$ for BDF2 and $\Delta t = \frac{1}{256}, \frac{1}{512}$ for AMB2. The relative errors are plotted in Figures 6.1–6.3. It is clear that although the errors grow initially, they remain bounded for all time. Moreover, the second-order in time accuracy for the velocity and the hydraulic head are also evident even in this onerous long-time experiment. The long-time accuracy for the pressure seems to be first-order in time, in agreement with our uniform in time error estimates. However, this is in contrast to the short-time second-order in time accuracy for p as recorded in Table 6.4.

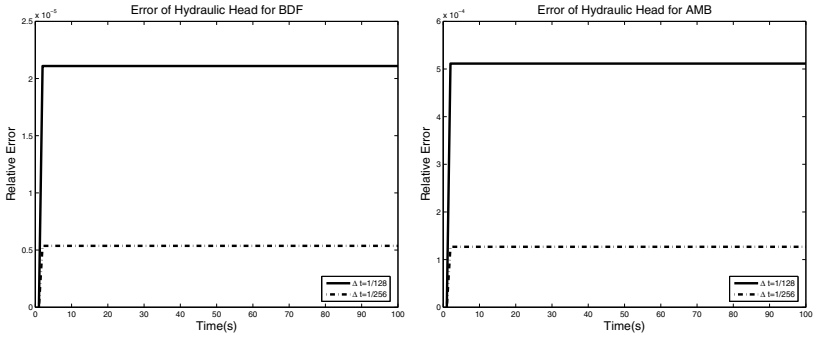

FIG. 6.1. *Relative error for ϕ in Example* 3 *for* BDF2 *(left) and* AMB2 *(right) up to $t = 100$ for $h = 1/64$.*

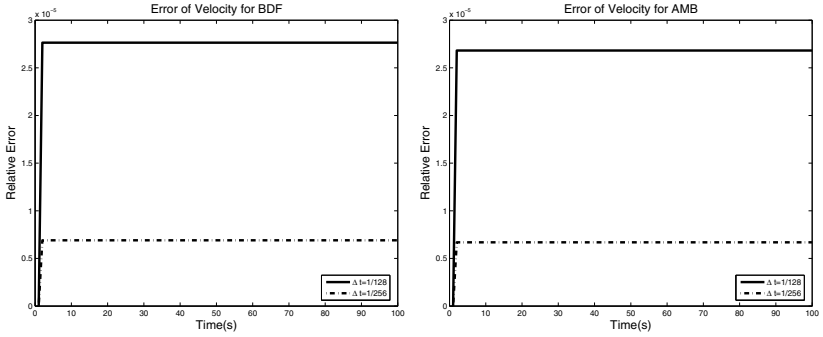

FIG. 6.2. *Same information as for Figure* 6.1 *but for $\mathbf{u}_f$.*

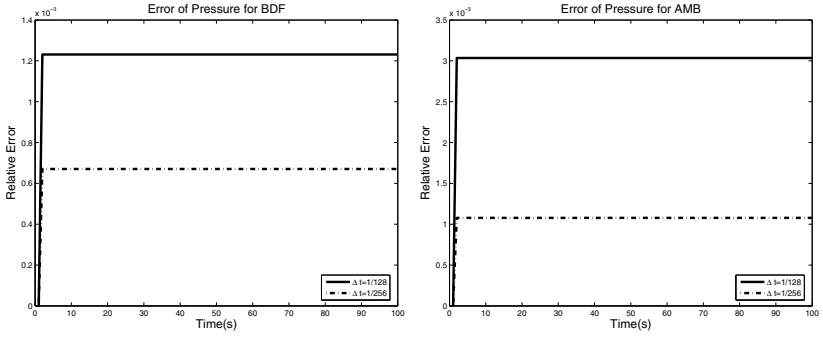

FIG. 6.3. *Same information as for Figure* 6.1 *but for p.*

Downloaded 03/17/23 to 131.151.26.204 . Redistribution subject to SIAM license or copyright; see https://epubs.siam.org/terms-privacy

Copyright © by SIAM. Unauthorized reproduction of this article is prohibited.

TABLE 6.4

Relative error and order of accuracy with respect to the spatial grid size h for Example 2 at $t = 1$ and with $\Delta t = h$.

	e_ϕ		$e_{\mathbf{u}}$		e_p	
h	BDF2	AMB2	BDF2	AMB2	BDF2	AMB2
1/16	2.05e-003	2.95e-002	1.49e-003	1.72e-003	4.88e-002	1.70e-001
1/32	4.36e-004	7.76e-003	4.18e-004	4.26e-004	1.40e-002	4.32e-002
1/64	9.84e-005	1.99e-003	1.09e-004	1.07e-004	3.64e-003	1.10e-002
1/128	2.32e-005	5.05e-004	2.75e-005	2.68e-005	9.29e-004	2.79e-003
r_{avg}	2.15	1.96	1.92	2.00	1.91	1.98

Example 3. To test the sharpness of time-step constraints for long-time stability, we set $\mathbf{f} = \mathbf{0}, f = 0$ and use the same initial conditions as for Example 1 [37],

$$\mathbf{u}_f(\mathbf{x}, 0) = \left([x^2(y-1)^2 + y] \ , \ \left[-\frac{2}{3}x(y-1)^3 + 2 - \pi \sin(\pi x) \right] \right),$$
$$\phi(\mathbf{x}, 0) = [2 - \pi \sin(\pi x)][1 - y - \cos(\pi y)],$$

and a consistent initial pressure. For the boundary conditions, homogeneous Dirichlet boundary conditions are imposed on the outside boundary $\partial\Omega_f \setminus \Gamma$ and $\partial\Omega_p \setminus \Gamma$. We set $K = 10^{-6}$ (the same as in [31] and $h = 1/20$, but change $\nu, S, \gamma_p, \gamma_f$) and observe the long-time behavior of $E = \|\vec{\mathbf{u}}\|^2$ up to time $T = 100$.

Figure 6.4 indicates that the time-step constraint is between 1/5 and 1/4 for the BDF2 scheme and between 1/12 and 1/9 for the AMB2 scheme. Here $\gamma_f = \gamma_p = g/5$. This setup is used as the base case for comparisons with subsequent tests.

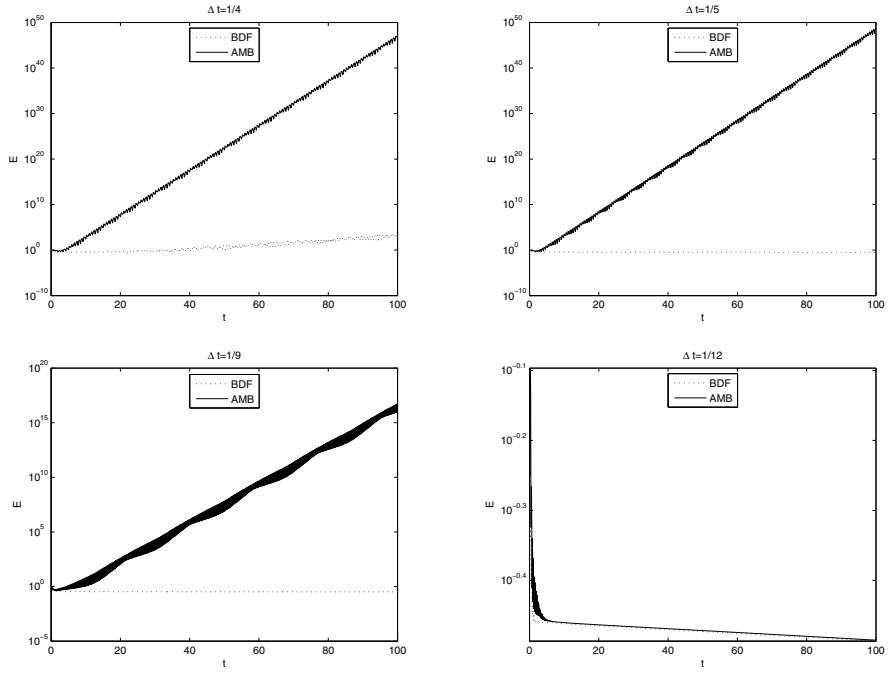

FIG. 6.4. *Energy E over time t. $\nu = S = g = \alpha_{BJSJ} = 1$, $\gamma_p = \gamma_f = g/5$, $K = 10^{-6}$, and $h = 1/20$.*

Copyright © by SIAM. Unauthorized reproduction of this article is prohibited.

Downloaded 03/17/23 to 131.151.26.204 . Redistribution subject to SIAM license or copyright; see https://epubs.siam.org/terms-privacy

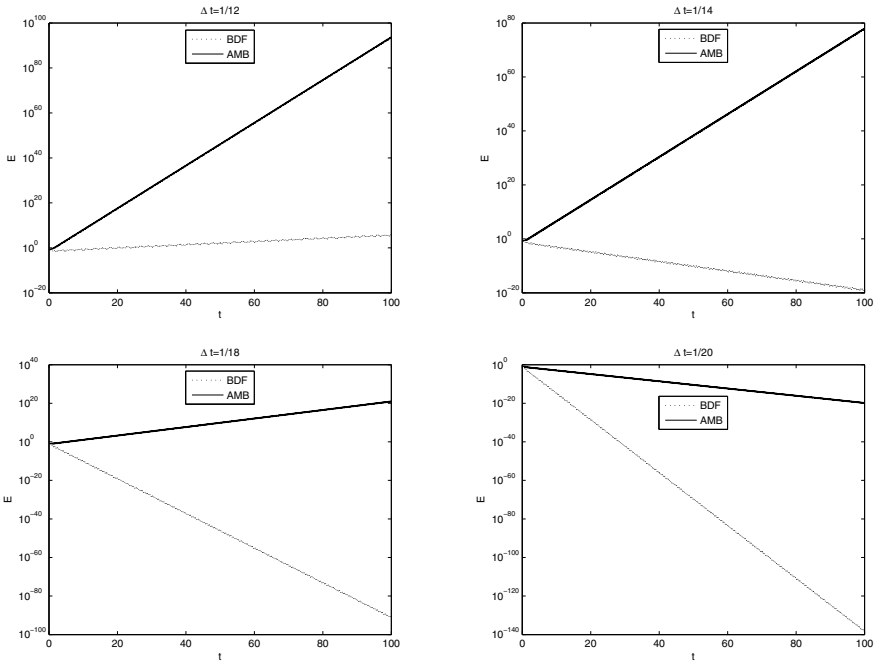

FIG. 6.5. *Energy E over time t. $S = 10^{-6}$, $\nu = g = \alpha_{BJSJ} = 1$, $\gamma_p = \gamma_f = g/5$, $K = 10^{-6}$, and $h = 1/20$.*

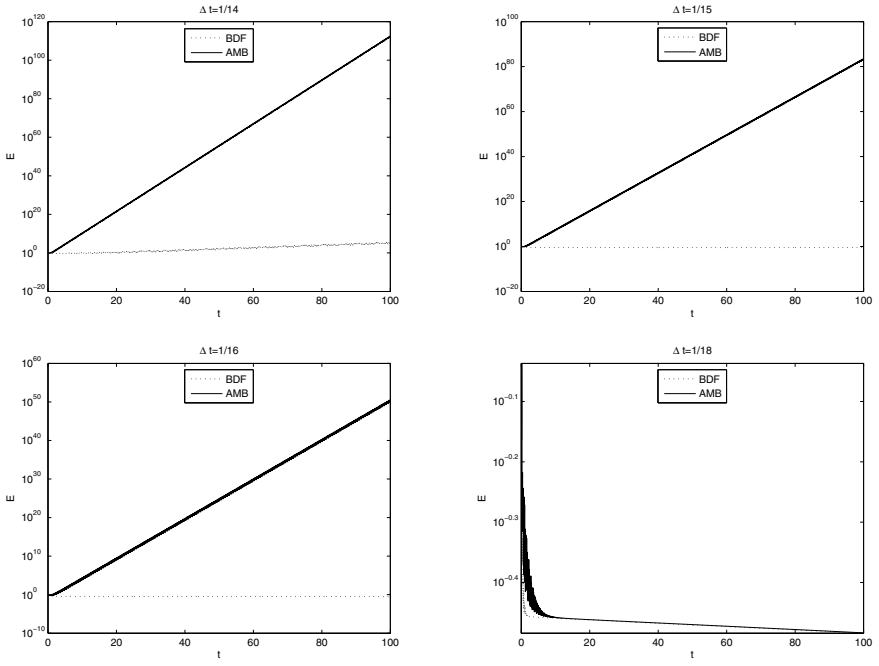

FIG. 6.6. *Energy E over time t. $\nu = S = g = \alpha_{BJSJ} = 1$, $\gamma_p = \gamma_f = g/10$, $K = 10^{-6}$, and $h = 1/20$.*

Copyright © by SIAM. Unauthorized reproduction of this article is prohibited.

Downloaded 03/17/23 to 131.151.26.204 . Redistribution subject to SIAM license or copyright; see https://epubs.siam.org/terms-privacy

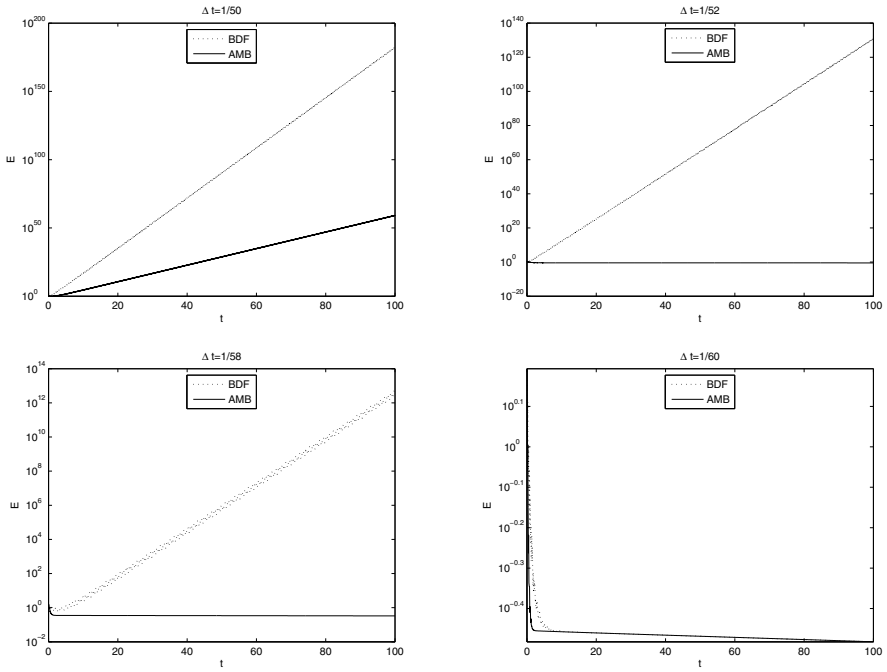

FIG. 6.7. *Energy E over time t.* $\nu = 10^{-1}$, $S = g = \alpha_{BJSJ} = 1$, $\gamma_p = \gamma_f = g/5$, $K = 10^{-6}$, *and* $h = 1/20$.

Figure 6.5 shows that the time-step constraint is between 1/14 and 1/12 for the BDF2 scheme and is between 1/20 and 1/18 for the AMB2 scheme with a smaller water storativity. Compared with Figure 6.4, it implies that smaller S requires more restrictive time-step constraints.

Figure 6.6 shows that the time-step constraint is between 1/15 and 1/14 for the BDF2 scheme and is between 1/18 and 1/16 for the AMB2 scheme with smaller coefficient for the artificial stabilizing terms. Compared with Figure 6.4, it implies that stronger stabilization relaxes time-step constraints.

Figure 6.7 shows that the time-step constraint is between 1/60 and 1/58 for the BDF2 scheme and is between 1/52 and 1/50 for the AMB2 scheme with a smaller ν. Compared with Figure 6.4, it implies that small ν leads to more restrictive time-step constraint consistent with our analysis.

7. Concluding remarks. We proposed and investigated two long-time accurate and efficient numerical methods for coupled Stokes–Darcy systems. The first is a combination of the BDF2 and the second-order Gear extrapolation method. The second is a combination of the second-order Adams-Moulton and Adams-Bashforth methods. Our algorithms are special cases of the IMEX schemes. The interfacial term that requires communication between the porous media and conduit, i.e., between the Stokes and Darcy components of the model, is treated explicitly in our algorithms so that only two decoupled problems (one Stokes and one Darcy) are solved at each time-step. Therefore these schemes can be implemented very efficiently and, in particular, legacy codes can be used for each component.

We have shown that our schemes are unconditionally stable and long-time stable in the sense that solutions remain uniformly bounded in time. The uniform bound in

Copyright © by SIAM. Unauthorized reproduction of this article is prohibited.

Downloaded 03/17/23 to 131.151.26.204 . Redistribution subject to SIAM license or copyright; see https://epubs.siam.org/terms-privacy

Downloaded 03/17/23 to 131.151.26.204 . Redistribution subject to SIAM license or copyright; see https://epubs.siam.org/terms-privacy

time of the solution leads to uniform in time error estimates. This is a highly desirable feature because the physically interesting phenomenon of contaminant sequestration and release usually occurs over a very long time scale and one would like to have faithful numerical results over such time scales. Spatial discretization is effected using standard FEMs. Time-uniform error estimates for the Darcy hydraulic head and the Stokes velocity and pressure for the fully discrete schemes are also presented. These estimates are illustrated by numerical examples. The methods proposed can also be utilized to approximate steady-state solutions in case the problem data are time independent. All these features suggest that the two methods have strong potential in real applications. Extended version of the current paper containing additional material can be found in [14].

On the other hand, there is still room for improvement. One could design even higher-order numerical methods. A third-order method was proposed in [10] without analysis. We are currently developing third-order unconditionally stable schemes based on the Adams–Moulton–Bashforth approach. It is also desirable to use different and adaptive time-steps for the two regions involved due to the disparate time scales in the two regions that one sees in practical situations; see, e.g., [34, 35]. Also, the mortar element method can be naturally adopted and may be useful to efficiently handle the different spatial scales in the two subdomains; see, e.g., [30, 21].

So far, all methods deal with confined (saturated) karst aquifers. Most aquifers are unconfined and hence different methodologies involving either two-phase flows or free boundaries must be considered. Models for unconfined karst aquifers are inherently nonlinear. Mathematical investigation of unconfined karst aquifers is still in its infancy and deserves much needed attention.

Last but not least, the application of these methods to the quantification of uncertainty in flow and contaminant transport would be of great interest in real applications that feature uncertainty in both the conduit geometry and matrix hydraulic conductivity.

REFERENCES

[1] G. Akrivis, M. Crouzeix, and C. Makridakis, *Implicit-explicit multistep finite element methods for nonlinear parabolic problems*, Math. Comp., 67 (1998), pp. 457–477.

[2] G. Akrivis, M. Crouzeix, and C. Makridakis, *Implicit-explicit multistep methods for quasilinear parabolic equations*, Numer. Math., 82 (1999), pp. 521–541.

[3] G. Akrivis and Y. Smyrlis, *Implicit-explicit BDF methods for the Kuramoto-Sivashinsky equation*, Appl. Numer. Math., 51 (2004), pp. 151–169.

[4] M. Anitescu, F. Pahlevani, and W. Layton, *Implicit for local effects and explicit for nonlocal effects is unconditionally stable*, Electron. Trans. Numer. Anal., 18 (2004), pp. 174–187.

[5] U. Ascher, S. Ruuth, and B. Wetton, *Implicit-explicit methods for time-dependent partial differential equations*, SIAM J. Numer. Anal., 32 (1995), pp. 797–823.

[6] G. Beavers and D. Joseph, *Boundary conditions at a naturally permeable wall*, J. Fluid Mech., 30 (1967), pp. 197–207.

[7] Y. Cao, M. Gunzburger, F. Hua, and X. Wang, *Coupled Stokes-Darcy model with Beavers-Joseph interface boundary condition*, Commun. Math. Sci., 8 (2010), pp. 1–25.

[8] Y. Cao, M. Gunzburger, B. Hu, F. Hua, X. Wang, and W. Zhao, *Finite element approximation of the Stokes–Darcy flow with Beavers–Joseph interface boundary condition*, SIAM J. Numer. Anal., 47 (2010), pp. 4239–4256.

[9] Y. Cao, M. Gunzburger, X. He, and X. Wang, *Domain decomposition method for Stokes-Darcy model with Beaver-Joseph interface condition*, Numer. Math., 117 (2011), pp. 601–629.

[10] Y. Cao, M. Gunzburger, X. He, and X. Wang, *Parallel, non-iterative, multi-physics domain decomposition methods for time-dependent Stokes-Darcy systems*, Math. Comp., accepted.

[11] A. Cesmelioglu, V. Girault, and B. Riviere. *Time-dependent coupling of Navier-Stokes and Darcy flows*, ESAIM Math. Model. Numer. Anal., 47, (2013), pp. 539–554.

Copyright © by SIAM. Unauthorized reproduction of this article is prohibited.

[12] W. Chen, P. Chen, M. Gunzburger, and N. Yan, *Superconvergence analysis of FEMs for the Stokes-Darcy System*, Math. Methods Appl. Sci., 33 (2010), pp. 1605–1617.
[13] W. Chen, M. Gunzburger, F. Hua, and X. Wang, *A parallel Robin–Robin domain decomposition method for the Stokes–Darcy system*, SIAM J. Numer. Anal., 49 (2011), pp. 1064–1084.
[14] W. Chen, M. Gunzburger, D. Sun, and X. Wang, *Efficient and long-time accurate second order methods for Stokes–Darcy system*, arXiv:1211.0567.
[15] P. Ciarlet, *The Finite Element Method for Elliptic Problems*, North-Holland, Amsterdam, 1978.
[16] M. Discacciati, E. Miglio, and A. Quarteroni, *Mathematical and numerical models for coupling surface and groundwater flows*, Appl. Numer. Math., 43 (2002), pp. 57–74.
[17] M. Discacciati and A. Quarteroni, *Analysis of a domain decomposition method for the coupling of Stokes and Darcy equations*, in Numerical Mathematics and Advanced Applications-ENUMATH 2001, F. Brezzi et al., eds, Springer-Verlag, Berlin, 2003, pp. 3–20.
[18] M. Discacciati, A. Quarteroni, and A. Valli, *Robin–Robin domain decomposition methods for the Stokes–Darcy coupling*, SIAM J. Numer. Anal., 45 (2007), pp. 1246–1268.
[19] M. Discacciati and A. Quarteroni, *Navier-Stokes/Darcy coupling: Modeling, analysis and numerical approximation*, Rev. Mat. Complut., 22 (2009), pp. 315–426.
[20] J. Frank, W. Hundsdorfer, and J. Verwer, *Stability of implicit-explicit linear multistep methods*, Appl. Numer. Math., 25 (1996), pp. 193–205.
[21] J. Galvis and M. Sarkis, *Non-matching mortar discretization analysis for the coupling Stokes-Darcy equations*, Electron. Trans. Numer. Anal., 26 (2007), pp. 350–384.
[22] V. Girault and P. A. Raviart, *Finite Element Methods for Navier-Stokes Equations: Theory and Algorithms*, Springer-Verlag, Berlin, 1986
[23] R. Glowinski, T. Pan, and J. Periaux, *A Lagrange multiplier/fictitious domain method for the numerical simulation of incompressible viscous flow around moving grid bodies:* I. *Case where the rigid body motions are known a priori*, C. R. Acad. Sci. Paris Sèr. I Math., 324 (1997), pp. 361–369.
[24] E. Hairer and G. Wanner, *Solving Ordinary Differential Equations* II*: Stiff and Differential-Algebraic Problems*, 2nd ed, Springer-Verlag, Berlin, 2002.
[25] W. Jäger and A. Mikelić, *On the interface boundary condition of Beavers, Joseph and Saffman*, SIAM J. Appl. Math., 60 (2000), pp. 1111–1127.
[26] I. Jones, *Low Reynolds number flow past a porous spherical shell*, Proc. Camb. Phil. Soc., 73 (1973), pp. 231–238.
[27] T. Kincaid, *Exploring the Secrets of Wakulla Springs*, Open seminar, Tallahassee, FL, 2004.
[28] M. Kubacki, *Uncoupling evolutionary groundwater-surface water flows using the Crank-Nicolson leapfrog method*, Numer. Methods Partial Differential Equations, 29 (2013), pp. 1192–1216.
[29] E. Kuniansky, *U.S. Geological Survey karst interest group proceedings*, in U.S. Geological Survey Scientific Investigations Report, Bowling Green, KY, 2008, pp. 2008–5023.
[30] W. Layton, F. Schieweck, and I. Yotov, *Coupling fluid flow with porous media flow*, SIAM J. Numer. Anal., 40 (2003), pp. 2195–2218.
[31] W. Layton, H. Tran, and C. Trenchea, *Analysis of long time stability and errors of two partitioned methods for uncoupling evolutionary groundwater-surface water flows*, SIAM J. Numer. Anal., 51 (2013), pp. 248–272.
[32] W. Layton, H. Tran, and X. Xiong, *Long time stability of four methods for splitting the evolutionary Stokes-Darcy problem into Stokes and Darcy subproblems*, J. Comput. Appl. Math., 236 (2012), pp. 3198–3217.
[33] W. J. Layton and C. Trenchea, *Stability of two IMEX methods, CNLF and BDF2-AB2, for uncoupling systems of evolution equations*, Appl. Numer. Math., 62 (2012), pp. 112–120.
[34] L. Shan, H. Zheng, and W. Layton, *A Non-iterative, Domain Decomposition Method with Different Time Step Sizes for the Evolutionary Stokes-Darcy Model*, Technical report, www.mathematics.pitt.edu/research/technical-reports.php (2011).
[35] L. Shan and H. Zheng, *Partitioned Time Stepping Method for Fully Evolutionary Stokes-Darcy Flow with Beavers-Joseph Interface*, Technical report, www.mathematics.pitt.edu/research/technical-reports.php (2011).
[36] M. Mu and J. Xu, *A two-grid method of a mixed Stokes-Darcy model for coupling fluid flow with porous media flow*, SIAM J. Numer. Anal., 45 (2007), pp. 1801–1813.
[37] M. Mu and X. Zhu, *Decoupled schemes for a non-stationary mixed Stokes-Darcy model*, Math. Comp., 79 (2010), pp. 707–731.
[38] A. Quarteroni and A. Valli, *Domain Decomposition Methods for Partial Differential Equations*, Oxford Science Publications, Oxford, UK, 1999.
[39] P. Saffman, *On the boundary condition at the interface of a porous medium*, Stud. Appl. Math., 1 (1971), pp. 77–84.

Downloaded 03/17/23 to 131.151.26.204 . Redistribution subject to SIAM license or copyright; see https://epubs.siam.org/terms-privacy

Copyright © by SIAM. Unauthorized reproduction of this article is prohibited.